Ocean Engineering 315 (2025) 119830

Contents lists available at ScienceDirect

Ocean Engineering

journal homepage: www.elsevier.com/locate/oceaneng

Research paper

Optimizing yaw angles for improved power generation in offshore wind farms: A statistical approach

Ignacio Formoso

Departamento de Sostenibilidad Ambiental, Instituto Tecnológico Centro Sur, Universidad Tecnológica (UTEC), Uruguay

ARTICLE INFO

Keywords:
Power loss mitigation
Wake effect analysis
Numerical optimization
Statistical modeling
Machine learning
Offshore wind power generation

ABSTRACT

Aerodynamic interactions among wind turbines diminish power generation in offshore wind farms. Adjusting a turbine's yaw angle, deliberately misaligned from the wind direction, mitigates energy losses from wake effects, thereby enhancing overall power generation. This study employs advanced wind farm simulation software for numerical simulations to compute the optimal yaw angle and associated percentage power gain for three offshore wind turbines under varying conditions, encompassing turbine models, wind speeds, turbulence intensities, and layouts. Two polynomial regression models and one decision tree classification model are developed to estimate the yaw angle and percentage power gain based on these conditions. These models are computationally efficient, integrating previously unconsidered predictors, and facilitating assessment of predictor impacts on yaw angle and power gain. Moreover, they enable real-time adjustment of turbine nacelle direction, positioning them for effective deployment at scale in offshore wind farms. Implementing these models is anticipated to extend and facilitate the use of turbine yawing as a strategy to enhance energy generation, providing computationally efficient tools for optimizing power generation in ocean wind farms.

1. Introduction

Active yaw control (AYC) involves deliberately misaligning the yaw direction of wind turbines from the wind direction to minimize energy losses caused by wake effects and reduce power production intermittency (Howland et al., 2019). In large-scale wind farms, these losses can be substantial, ranging from 30% to 40% (Zong and Enbo, 2022). Implementing AYC has shown promise in optimizing power generation across wind farms by increasing the power output of turbines (Stanley et al., 2023). AYC is recognized for its effectiveness in mitigating wake effects and is established as a leading wake redirection strategy (Zong and Porté-Agel, 2021), proving to be a more effective control technique compared to conventional greedy control (Kim et al., 2023), where each turbine focuses solely on maximizing its own power production.

Extensive research on the effect of AYC on power gain encompasses various numerical approaches, including both low-fidelity and high-fidelity models for simulating wind wakes generated by turbines. Computational studies, such as those by Wei et al. (2023) and Xin et al. (2022), have employed Large Eddy Simulations (LES) to investigate AYC under different conditions. Ciri et al. (2018) and Bempedelis et al. (2023) also utilized LES to study the impact of turbine scale and wake steering effects, respectively. Archer and Vasel-Be-Hagh (2019) concluded that positive yaw misalignment angles lead to net power gains in a wind farm, while negative angles result in losses. Additionally, Das and Shen (2023) conducted a computational investigation of a three-by-three wind turbine array using LES to explore wind farm behavior under varying wind conditions and yaw angles. They concluded that wind speed has a limited impact on wake characteristics and power outputs, except at lower wind speeds with a yaw angle of 20 degrees. Kuo et al. (2020) used an analytical wake model to optimize yaw angles, observing that higher power density increases potential production improvement through yaw optimization. P. Fleming and colleagues have combined computational simulations with experimental validation to study wake steering performance using various strategies (Stanley et al., 2023; Annoni et al., 2018; Fleming et al., 2022; Stanley et al., 2022; Simley et al., 2021; King et al., 2021; Fleming et al., 2021).

Table 1 summarizes the effectiveness of AYC as a function of relevant parameters in previous works and the current study. The parameters include the distance between wind turbines (d), the turbine rotor diameter (D), the wind velocity (U), and the wind turbulence intensity (I). Turbine distance was considered to increase either with increasing streamwise or spanwise turbine spacing. Up arrows indicate that AYC is more effective as the parameter increases, down arrows indicate the opposite, an equality symbol indicates no efficiency change as the parameter increases, and a dash indicates that the study did not state the relationship between AYC efficiency and the parameter. The number of turbines and the methods used in the studies are also presented. This

E-mail address: ignacio.formoso@utec.edu.uy.

https://doi.org/10.1016/j.oceaneng.2024.119830
Received 20 June 2024; Received in revised form 16 November 2024; Accepted 17 November 2024

Table 1
Effectiveness of AYC as a function of key parameters in previous works and the current study: turbine distance (d), rotor diameter (D), wind velocity (U), and turbulence intensity (I).

Study	No. turbines	Methods used	Effectiveness of AYC			
			d	D	U	I
Zong and Porté-Agel (2021)	3	Wind tunnel experiments, Analytical wind farm model	↓	–	–	↓
He et al. (2024)	5	Analytical wind farm model	↓	–	–	↓
Wei et al. (2023)	3	Large-eddy simulations	↑ ↓[a]	–	↓	↓
Stanley et al. (2022)	10–50	Analytical wind farm model	↓	–	–	–
Ciri et al. (2018)	3	Large-eddy simulations	–	↑	–	–
Das and Shen (2023)	9	Large-eddy simulations	–	–	=[b]	–
Kuo et al. (2020)	39	Analytical wind farm model	↓	–	–	–
Bastankhah and Porté-Agel (2019)	5	Wind tunnel experiments	↓	–	–	↓
This study	2	Analytical wind farm model, Linear regression model	↓	↑	↓	↓

[a] Increasing then decreasing.
[b] Except for lower wind speeds at a yaw angle of 20 degrees.

table shows that the present study encompasses all relevant parameters affecting the effectiveness of AYC, making it more comprehensive than previous studies, with which it presents a good qualitative agreement. This thorough parametric study was possible due to the simplicity and low computational cost of the models developed for calculating the optimal yaw angle and percentage power gain from applying AYC.

Despite the advances and insights provided by past research, no statistical model incorporating multiple relevant predictors has been developed to offer deeper insights into the effects of wake steering on power generation. Such a model could serve as a tool for the rapid optimization of wind turbine yaw angles. Hence, this article utilizes statistical regression analysis to develop a model that introduces a novel approach for fast and scalable optimization in wake steering. The computational efficiency of analytical and statistical models employed in wake steering is critical for optimizing controller design and the operation of online control systems (Fleming et al., 2021).

This study examined a layout with two turbines, where the second turbine was intentionally placed in aerodynamic interference with the wake of the first. Numerous numerical simulations were conducted using the FLOw Redirection and Induction in Steady State (FLORIS) software, combined with the Grid Search (GS) optimization method, to determine the optimal yaw angle for the wind turbine and the associated power gain from controlling this angle. Based on the simulation results, three numerical models were developed to estimate the optimal yaw angle for the upstream turbine and the corresponding power gain for the pair, considering wind speed, turbulence intensity, rotor diameter, nominal wind turbine speed, and layout.

A decision tree-based classification model was developed to identify the operating conditions under which wake control is beneficial. Additionally, two multiple linear regression models were fitted: one to calculate the optimal yaw angle of the upstream wind turbine for maximizing power generation by the turbine pair, and another to determine the percentage power gain associated with controlling this angle. The results indicated that both the classification model and the yaw angle model provide relatively accurate estimates. However, while the percentage power gain model follows the simulation trends, it exhibits higher errors, making it suitable for qualitative analysis but not for predictive purposes. The models were capable of making a single prediction in tenths of a second, making them potentially scalable with the number of turbines, as pursued in wake steering control applications (Fleming et al., 2022).

2. Numerical procedure

This section outlines the numerical procedure employed in this study. Firstly, the selected predictors for the numerical models are presented, detailing their respective variation intervals. These predictors serve as independent variables defining the operating conditions simulated in this research. Secondly, the numerical simulations conducted using the FLORIS software are described. These simulations aim to determine the optimal yaw angle of the upstream wind turbine and quantify the percentage power gain for the pair of wind turbines operating under conditions of aerodynamic interference. In this study, FLORIS is used primarily to generate the initial data required for developing the statistical yaw angle and power gain models, serving as a foundational tool. Thirdly, the classification and regression models are developed based on the simulation results, which are subsequently discussed. The primary contribution of this article lies in the development and implementation of these surrogate models. Once established, these models can predict the optimal yaw angles and power gains without further reliance on FLORIS. Fourthly, a sensitivity analysis is conducted to identify the most relevant parameters affecting the turbine's optimal yaw angle and power gain. Finally, the model responses are compared with those from the simulations in three canonical cases.

Fig. 1 provides a summarized depiction of the procedural steps involved in developing the models utilized for wake steering optimization and analysis. Section numbers are referenced within each block of the diagram.

2.1. Selected model predictors

This study focuses on an array of two wind turbines, denoted as T1 and T2, where T2 is positioned downstream of T1 and exposed to the wake of T1. Fig. 2 illustrates the wind turbine layout and highlights the key parameters under investigation. The yaw angle of T1 (γ) plays a critical role in regulating the power output of both turbines. To determine the optimal yaw angle γ^* of T1 that maximizes the combined power generation and to assess the percentage power gain (ΔP) achieved through γ control, a set of predictors was selected, including airflow characteristics, wind turbine specifications, and layout parameters. In FLORIS, the selected adjustable parameters used as predictors encompass wind speed at turbine T1 (U), coordinates of turbine T2 in both streamwise (x) and spanwise (y) directions relative to T1, free-stream turbulence intensity (I), rotor diameter (D), and nominal wind turbine speed (U_r).

Since a change in wind direction is equivalent to changing the relative coordinates x and y of T2, and these coordinates are already considered in the study, it is not necessary to account for wind direction explicitly. However, wind direction is crucial for studying yaw control strategies for specific farm sites and layouts (Song et al., 2023; Kuo et al., 2020). In these problems, the use of AYC is integral to the co-design of control systems, where optimizing park layout incorporates actions to control wake effects (Stanley et al., 2023; Song et al., 2023).

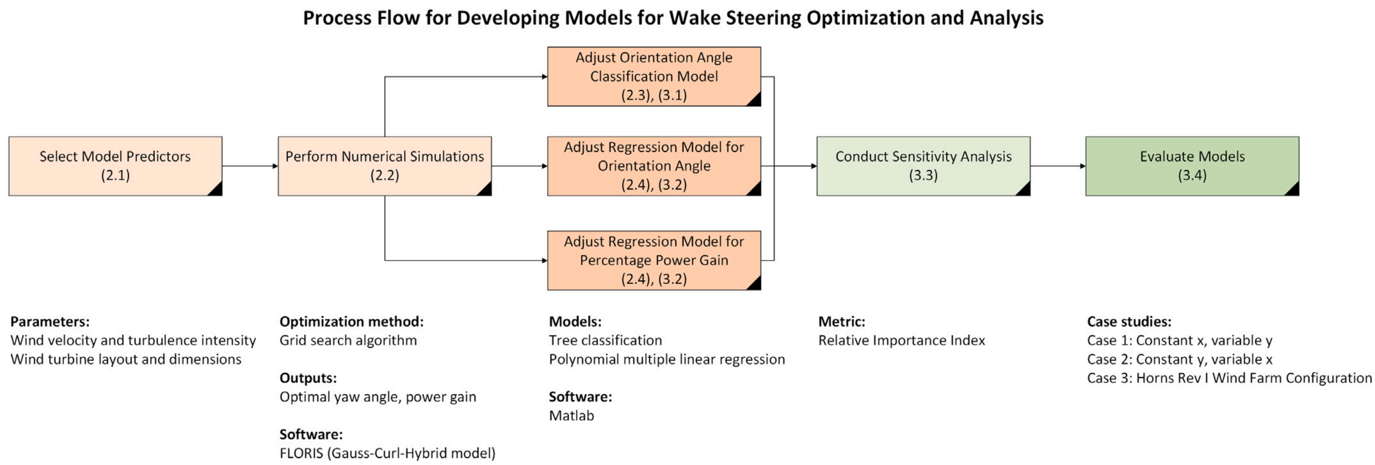

Fig. 1. Block diagram illustrating the procedural flow for developing the models utilized in wake steering optimization and analysis.

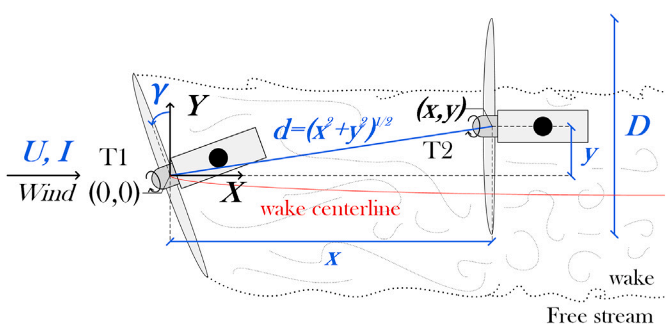

Fig. 2. Sketch of the wind farm layout (not to scale) depicting the main parameters considered in this study.

This comprehensive set of field-measurable predictors enables real-time calculation of model responses, facilitating dynamic control of power generation for both turbines. It is important to note that this study focuses solely on the immediate downstream turbine (T2) without considering impacts on turbines further downstream. This narrow focus allows for a detailed examination of the direct interactions between T1 and T2 within the specified experimental conditions. Numerous studies have highlighted the significant impact of these parameters on wind turbine power output in scenarios involving aerodynamic interactions. For instance, Xin et al. (2022) conducted LES on a wind farm with two NREL 5 MW reference turbines, varying turbine spacing from $5D$ to $8D$ and applying yaw control to the upstream turbine. Their findings underscore a strong correlation between total power output, yaw control, and turbine spacing. Similarly, Zong and Enbo (2022) identified streamwise turbine spacing, turbulence intensity, and wind speed as crucial factors influencing net power gain in studies involving active wake control strategies. Additionally, wind speed is recognized for its significant impact on wake control efficiency (Simley et al., 2021).

Firstly, in defining the range of variation for the coordinate x, the objective was to position T2 within the wake generated by T1, considering that within a wake length, the velocity typically recovers to approximately 90% of its initial value (Stegner et al.). For a 5% turbulent intensity of the free stream, the wake extends between 12–13 rotor diameters, and for a 25% turbulent intensity, it extends between 4–6 rotor diameters (Stegner et al.), with an average wake length of 10 diameters. Accordingly, the coordinate x was varied between 5 and 10 rotor diameters, aligning with the standard turbine spacing in the streamwise direction, typically ranging from 6 to 10 turbine diameters (Stegner et al.). For the coordinate values of y, a maximum spanwise displacement of 1 rotor diameter for turbine T2 was considered on each side of T1, consistent with the spacing used in the experimental analysis of Ref. Zong and Porté-Agel (2021). This choice resulted in a substantial range of layouts where aerodynamic interference between T1 and T2 occurs.

Secondly, the rotor diameters used in the simulations were obtained from three offshore turbine models available in FLORIS, whose characteristics are summarized in Table 2. These turbines cover a significant range of power outputs.

Thirdly, wind speed values ranging from 5 m/s to 25 m/s were chosen to encompass nearly the entire operational range of the turbines listed in Table 2. Turbulent intensity, varying between 5% and 15%, was also selected to cover conditions from low to moderate turbulence, reflecting the influence of multiple factors such as elevation and terrain roughness on this parameter. The specific values assigned to the predictors are summarized in Table 3.

Moreover, to streamline the presentation of results, the predictors were further condensed into four dimensionless parameters, as shown in Eq. (1):

$$y' = \frac{y}{x},\ U' = \frac{U}{U_r},\ d' = \frac{d}{D},\ I \tag{1}$$

where $d = \sqrt{x^2 + y^2}$ denotes the distance between the wind turbines.

2.2. Numerical simulations

FLORIS is an open-source computational aerodynamics modeling program specifically designed for wind farm energy production estimation. It integrates wake models to simulate the interaction between wind turbines operating under steady-state conditions. By computing the velocity field within the wind farm, FLORIS calculates power output. The models in FLORIS typically combine velocity deficit and wake deflection models. One extensively utilized model in wake effect studies is the Jensen model (Jensen, 1983), which has been employed by various researchers for optimizing turbine wake steering (Stanley et al., 2023, 2022). In the Jensen velocity deficit model, the wake velocity deficit is assumed constant within the wake, extending linearly downstream, and wake deflection is modeled using the Jiménez model (Jiménez et al., 2010). However, this model tends to overestimate power generation under full wake interference and underestimate it under partial wake interference conditions (Niayifar and Porté-Agel, 2016).

Accurate wake effect representation is essential for effective real-time wind farm control (Amiri et al., 2024). The Gauss-Curl-Hybrid (GCH) model in FLORIS, used in this study, assumes flow-conserving

Table 2
Characteristics of the wind turbines considered in the study.

Model	H [m]	D [m]	U_r [m/s]	U_a [m/s]	U_c [m/s]	P_r [MW]	Reference
NREL 5 MW	90	126	11.4	3	25	5	Jonkman et al. (2009)
IEA 10 MW	119	198	11.0	4	25	10	Gaertner et al. (2020)
IEA 15 MW	150	240	10.6	3	25	15	Gaertner et al. (2020)

Table 3
Values assigned to the predictors in the study.

Predictor	x [m]	y [m]	U [m/s]	I [%]
Value	$5D, 6D, \ldots, 10D$	$-D, -0.75D, \ldots, D$	$5, 7.5, \ldots, 25$	$5, 10, 15$

Table 4
Wake and deflection parameters for the Gauss-Curl-Hybrid model.

Parameter	k_a	k_b	α	β	ϵ	ϕ
Value	0.380	0.004	0.580	0.077	0.2 D	2.000

self-similarity and integrates findings from various studies (Bastankhah and Porté-Agel, 2016; Niayifar and Porté-Agel, 2016; King et al., 2021). It incorporates effects like air drag, wake asymmetry, and secondary wake direction, and models wake velocity deficit with a Gaussian distribution, accounting for increased turbulence intensity due to turbine interactions. This results in a velocity deficit distribution that aligns better with theoretical and experimental observations (Amiri et al., 2024). The GCH model has been utilized in studies such as Stanley et al. (2022) and Fleming et al. (2021) to model wake steering in wind farms and calculate power gain. It is specifically designed to incorporate the secondary effects of wake steering in turbine arrays and has shown good agreement with LES results across diverse scenarios, as detailed in King et al. (2021). In that work, the GCH model was compared with LES for both 3- and 5-turbine arrays, with turbine spacings of 7D and 6D, respectively, under turbulence intensities of 6% and 10%. The percentage power gains obtained from implementing yaw control were found to be reasonably close between the FLORIS GCH model and the LES results. This validation underscores the GCH model's reliability as a wind farm simulation tool, particularly in accurately modeling wind wakes in the far wake region produced by turbines operating under yawed conditions.

The GCH model includes several configurable parameters, which for this study have been maintained at their default values as specified in FLORIS. These default values are consistent with those used in optimization studies of wake steering, such as the one detailed by Gori et al. (2023), and are summarized in Table 4. The use of default parameters from the Gaussian-shaped wake deficit model led to a very good agreement with historical data for most wind directions across three offshore wind farms. However, a larger discrepancy was observed in centrally positioned turbines in the largest wind farm, where deep-array effects are more pronounced (Doekemeijer et al., 2022). In the GCH model, parameters like k_a and k_b adjust turbulence intensity and wake recovery, while α and β govern turbulence and thrust coefficient influence on near-wake length. Additionally, ϵ defines vortex core size, and ϕ incorporates yaw-enhanced mixing turbulence (Gori et al., 2023). For illustrative purposes, Fig. 3 depicts a simulation using the GCH model with parameters set to: $x = 5D$, $y = 0.5D$, $D = 198$ m, $\gamma = 18°$, $U = 11$ m/s, $U_r = 11$ m/s, and $I = 5\%$. As stated in Archer and Vasel-Be-Hagh (2019), Fig. 3 demonstrates that the wake is deflected from its axis by an angle opposite to the yaw misalignment angle.

The simulations were conducted using a full factorial experimental design, where each combination of predictor values from Table 3 was tested, resulting in 4374 instances. Grid Search (GS) optimization was performed in each run to determine the optimal yaw angle of T1 (γ^*) and the percentage increase in power (ΔP) for both T1 and T2 through AYC. Several other optimization algorithms have been used in numerical studies to compute the optimal yaw angle for maximizing power production. Traditional methods like Sequential Least Squares Programming (SLSQP) require extensive computational resources and scale exponentially with the number of turbines, making them inefficient for large farms (Fleming et al., 2022). Heuristic methods, such as the Serial-Refine method, achieve comparable power generation levels with significantly less computational effort and linear scaling (Stanley et al., 2023; Fleming et al., 2022; Stanley et al., 2022). Random Search (RS) (Kuo et al., 2020), Particle Swarm Optimization (PSO) (Song et al., 2023), Bayesian Optimization (BO) (Bempedelis et al., 2023), and analytical gradient methods (Howland et al., 2019; Ciri et al., 2018) have also been employed for this objective. Despite the computational intensity of brute-force methods like GS, this approach was chosen due to its ability to comprehensively evaluate all potential parameter combinations at the initial stage of data gathering for subsequent statistical modeling.

Consistent with prior research (Xin et al., 2022; Stanley et al., 2022; Lin and Porté-Agel, 2020), yaw angles (γ) were varied from 0 to 30 degrees in increments of 1 degree. Here, 0 degrees indicates that the turbine rotor is aligned directly with the incident wind. In FLORIS, γ represents the angle between the turbine rotor axis and the incident wind direction in the horizontal plane. Only positive yaw angles were considered due to increased mechanical loads with negative angles (Stanley et al., 2022; Fleming et al., 2014) and minimal differences in power production between positive and negative angles (Zong and Porté-Agel, 2021). Positive yaw angles (counter-clockwise rotation) are also found to be more beneficial than negative angles (Archer and Vasel-Be-Hagh, 2019). See Fig. 2 for illustration. Though AYC for T2 might boost total power output, empirical evidence suggests minimal gains (Wei et al., 2023; Bastankhah and Porté-Agel, 2019). Optimal yaw distributions typically decrease from upstream to downstream turbines (Kuo et al., 2020), with downstream turbines ideally aligned perpendicular to the flow (Bastankhah and Porté-Agel, 2019). Thus, T2's rotor orientation was fixed perpendicular to the flow in all simulations.

The wind is assumed to flow from left to right, in an easterly direction, corresponding to a 270° angle measured clockwise from the vertical in FLORIS. The atmospheric boundary layer is modeled using a power law with an exponent of 0.12, appropriate for neutrally stable atmospheric conditions over open water. For all calculations, wind direction is assumed to remain constant with height, disregarding any wind veer. The mean turbine velocity is calculated using FLORIS's default method, which employs a cubic average based on wind velocities sampled across a 3 × 3 grid positioned over the rotor's swept area. The air density is assumed to be 1.225 kg/m^3, which corresponds to standard atmospheric conditions.

2.3. Adjustment of the yaw angle classification model

To determine scenarios where adjusting the yaw angle of T1 enhances overall power generation, a decision tree classifier model was tailored for this purpose. To keep the model simple, a maximum of 10 splits was established. This machine learning approach is widely adopted for classification tasks in wind energy studies. The criterion for reorienting T1 was set based on a minimum threshold of a 1% increase in power generated by the turbine pair. Specifically, if the calculated ΔP exceeds this threshold, reorienting T1 is deemed beneficial; otherwise, T1 remains at $\gamma = 0°$, directly facing the wind. The classifier's response is formulated as a function of the predictors defined in Eq. (1), articulated as follows:

$$\gamma_b = \gamma_b \left(y', U', d', I \right) \tag{2}$$

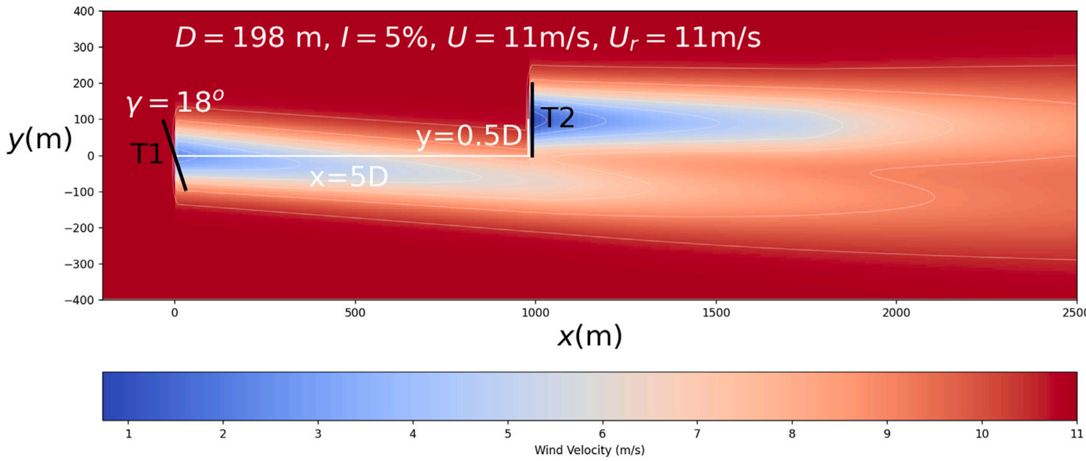

Fig. 3. Simulated velocity field at turbine hub-height (horizontal cut) using FLORIS Gauss-Curl-Hybrid model.

Here, γ_b denotes the binary output of the model, where it outputs 0 when reorientation of T1 is not justified, and 1 otherwise. Certain combinations of wind conditions, wind turbine models, and layouts demonstrate an advantageous increase in power generation by T2, more than compensating for any reduction in T1's output. In contrast, in other scenarios, the reorientation of T1 does not yield sufficient benefit to justify the adjustment. The use of the classification model was integral to refining and validating the approach, ensuring robust control over T1's orientation while minimizing unnecessary turbine adjustments that yield insignificant power gains. All simulations conducted were considered in the adjustment. Hereafter, this classification model will be denoted as M0.

2.4. Adjustment of regression models for yaw angle and percentage power gain

To estimate the optimal yaw angle of T1 and the percentage power gain associated with both T1 and T2, two polynomial regression models of multiple linear form were fitted to the data obtained from the simulations. Prior to fitting the models, simulations were discarded where the percentage increase in generated power was less than 1%, retaining only those where $\Delta P > 1\%$, as these were the cases of interest. As a result, 543 simulations were considered in the fitting, representing approximately 12% of the total.

The method used to fit both models was stepwise regression, employing a forward selection procedure. This procedure began with a constant initial model and gradually added the most significant terms at each step. The addition of terms ceased when all variables not included in the model had p-values greater than 0.05, ensuring the relevance of the predictors. Since terms of order higher than quadratic did not significantly improve the goodness of fit for the optimal yaw angle model, only linear, quadratic, and interaction terms were considered. However, for the percentage power gain model, linear, quadratic, cubic, and interaction terms were included.

Firstly, a linear regression model was considered to adjust the optimal yaw angle of T1 based on the predictors presented in Eq. (1), given by Eq. (3):

$$\gamma^* = \gamma^*\left(y', U', d', I\right) \tag{3}$$

A higher value of γ^* indicates a greater need to divert the wake generated by T1, avoiding (or reducing) aerodynamic interference with T2, in order to maximize the power produced by the pair of wind turbines. Hereafter, the regression model for γ^* will be referred to as M1.

Secondly, a linear regression model was considered to adjust the percentage power gain linked to active yaw control, given by Eq. (4):

$$\Delta P = \Delta P\left(y', U', d', I\right) \tag{4}$$

Table 5
Predictors, optimal yaw angle of T1, and power gain by T1 and T2 in four representative instances out of the 543 used to fit the regression models.

Instance	y'	U'	d'	I [%]	γ^* [°]	ΔP [%]
1	−0.0500	1.1364	5.0062	5	30	2.60
2	0.0000	0.4545	5.0000	5	24	12.73
3	0.0000	0.6818	5.0000	5	29	8.85
...	...	...	...	...	...	...
543	0.1071	0.4386	7.0401	15	9	1.35

A higher value of ΔP indicates a greater power gain for T1 and T2 resulting from the control applied to γ, calculated as shown in Eq. (5):

$$\Delta P = 100\frac{P_{\gamma^*} - P_0}{P_0}\% \tag{5}$$

Here, P_{γ^*} and P_0 represent the power generated by T1 and T2 with $\gamma = \gamma^*$ and $\gamma = 0^o$, respectively. This metric of power output improvement, defined in Eq. (5), is analogous to the one used by Bempedelis et al. (2023), where both high-fidelity and low-fidelity wake models were employed to investigate wake steering effects in a wind farm, and to the one used by He et al. (2024) to study wake steering strategies for combined power enhancement and fatigue mitigation within wind farms. It quantifies the percentage improvement relative to the non-yawed scenario. Henceforth, the regression model for ΔP will be denoted as M2.

Since the response of the classification model is essential for guiding the estimation of γ^* and ΔP under specific operating conditions, using model M0 before models M1 and M2 is required.

3. Results and discussion

Table 5 presents the values of the predictors, the optimal yaw angle of T1, and the percentage increase in power generated by T1 and T2, both calculated with FLORIS, for four representative instances out of the 543 used to fit the regression models.

The optimal yaw angle of T1 and the percentage power gain of T1 and T2 associated with active yaw control, as obtained in the simulations, are detailed in the penultimate and last columns of Table 5, respectively. Specifically, the optimal yaw angle γ^* ranged from 6° to 30°, and the percentage power gain ΔP varied from 1.0% to 25.6%, with an average of approximately 6%. These results are consistent with findings from an experimental study (Ozbay et al., 2012), which observed similar efficiency gains for tandem turbines with a downstream distance of $x/D = 2$ and yaw control on the upstream turbine.

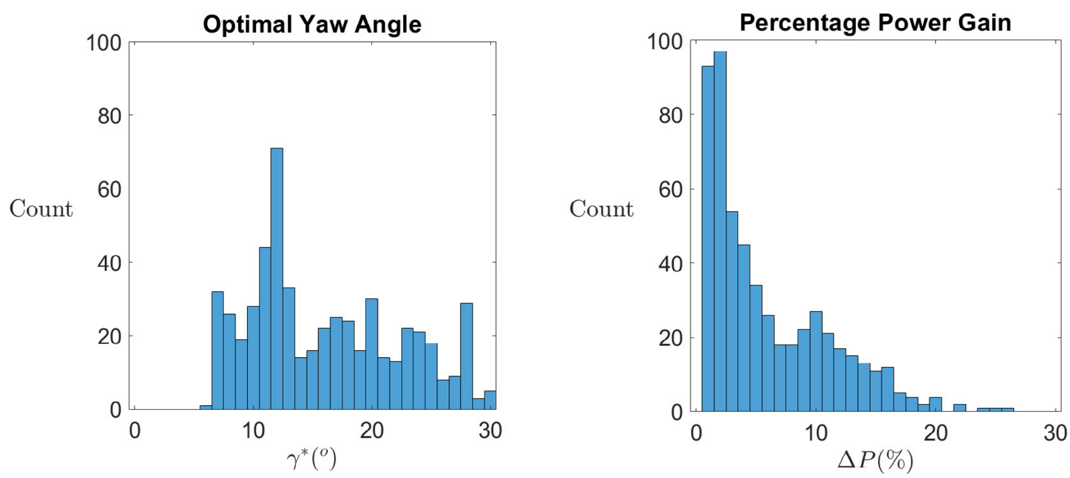

(a) (b)

Fig. 4. Histograms of simulation results: (a) Optimal yaw angle, (b) Percentage power gain.

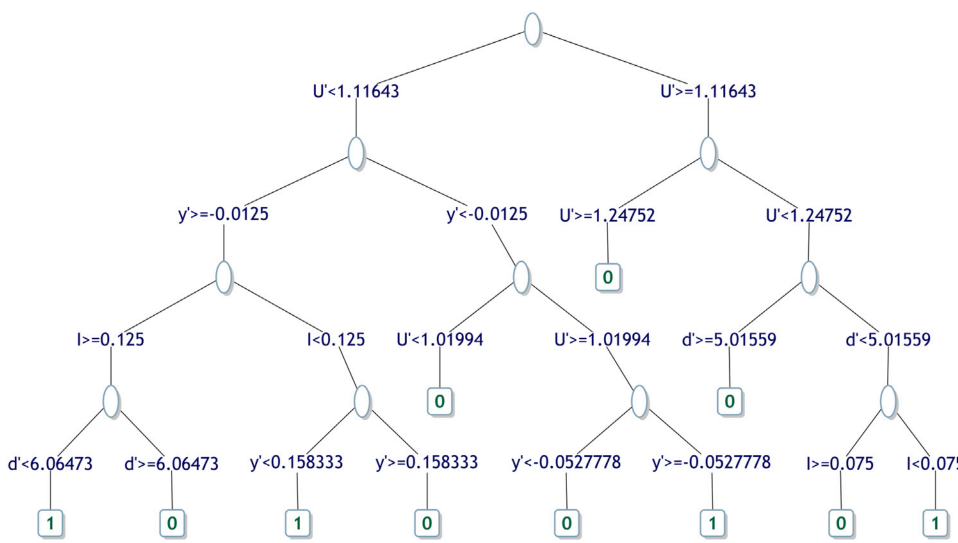

Fig. 5. Graphical representation of the fitted decision tree, generated using the Cmap software.

Additionally, field tests by the National Renewable Energy Laboratory and Stanford University reported that active yaw control can increase total wind farm power production by 5%–15% when wind directions are aligned with turbine rows (Zong and Enbo, 2022). Similarly, Bastankhah and Porté-Agel (2019) found that yaw control can enhance overall wind farm efficiency by up to 17% compared to non-yawed conditions, aligning with the findings of this study.

The relatively low mean value of the power gain compared to the maximum achieved suggests that while certain operating conditions allow for significant power increases, even exceeding 20%, in most cases, the gain obtained through active yaw control is relatively modest, typically only a few percentage points. Figs. 4(a) and 4(b) present histograms of the optimal yaw angles and percentage power gains, respectively, with a bin width of one degree. Fig. 4(a) shows that yaw angles between 0 and 5 degrees were not used, with angles of 11° and 12° being predominant. Fig. 4(b) indicates that, in most runs (approximately 53%), the power gain was below 5%. However, within a wind farm consisting of numerous turbines, even a modest percentage gain can result in a significant increase in energy production. This underscores the importance of implementing appropriate control strategies, as such gains can be achieved without the need for new technologies or costly infrastructure investments.

Next, the results obtained with the classification model, M0, and the regression models, M1 and M2, are presented and analyzed. All three models were developed using Matlab software.

3.1. Yaw angle classification model

Fig. 5 shows the graphical representation of the fitted tree classification model, while Fig. 6 displays its confusion matrix. With an accuracy rate of 96.11% and an error rate of 3.88%, the model demonstrates excellent classification performance. The matrix reveals that out of the 3831 instances where $\Delta P < 1\%$ (True = 0) was observed in the simulations, the model misclassified 152 instances. Similarly, out of the 543 instances where $\Delta P > 1\%$ (True = 1) was observed, it misclassified 18 instances.

Fig. 7 presents a parallel coordinates plot showing the classification results of the simulations. Each axis represents a predictor scaled to its range of values. Simulations classified with $\gamma_b = 1$ (Response = 1) are depicted in orange, while those classified with $\gamma_b = 0$ (Response = 0) are shown in blue. This visualization provides insights into the conditions under which redirecting the wake generated by T1 is justified. Firstly, it emphasizes the importance of this redirection when the spanwise coordinate, y, is positive, as depicted in Fig. 2. In such cases, T1's

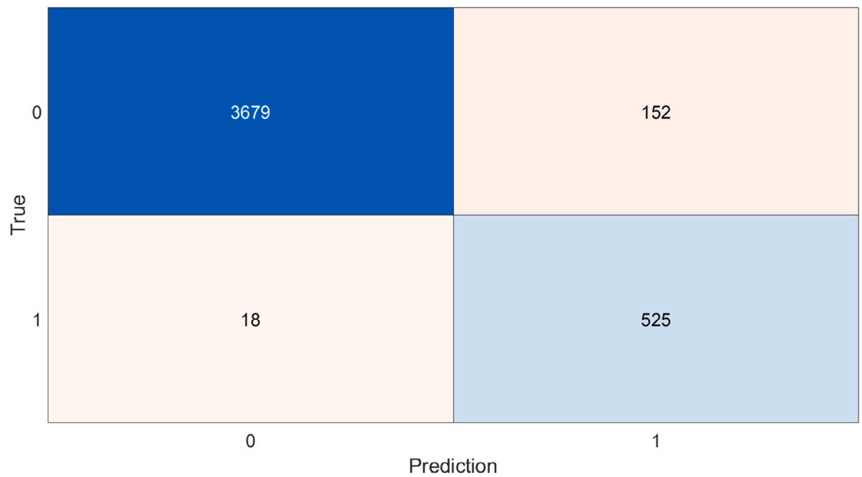

Fig. 6. Confusion matrix of the classification model.

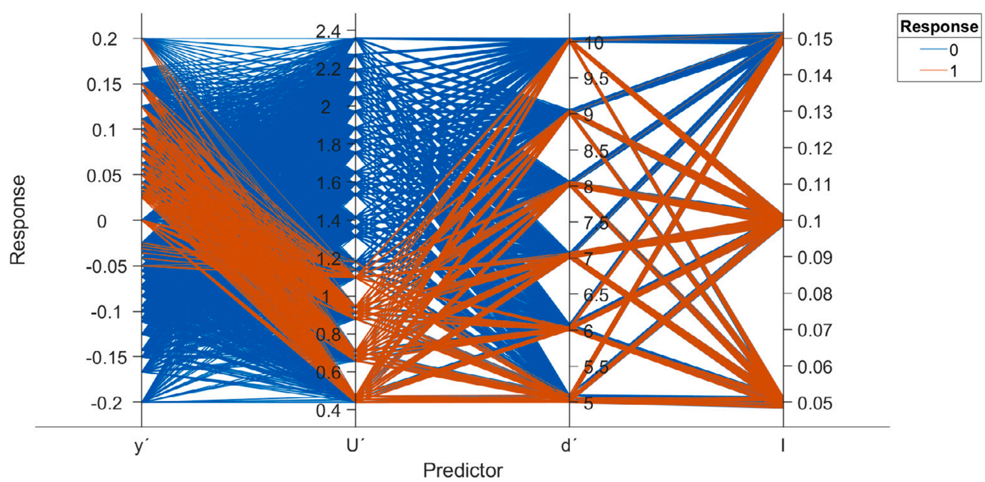

Fig. 7. Parallel coordinates plot of the classification model.

ability to mitigate aerodynamic interference with T2 is enhanced by restricting its rotation to positive γ angles, facilitating clockwise wake deflection, as illustrated in Fig. 3. Secondly, it is inferred that reorienting T1 is advantageous when the wind speed remains below a specific percentage of the nominal wind turbine speed, particularly 120% or $U' < 1.2$, due to the slower recovery of the velocity deficit in the wake region compared to higher wind speeds. Thirdly, since the number of orange lines decreases as the value of d' increases, it is inferred that the closer T1 and T2 are, the more necessary it becomes to control the orientation of T1. This is a sensible observation because the smaller the distance between the wind turbines, the greater the expected deficit in wind speed incident on T2 caused by the wake effect. However, even at moderate distances of the order of ten rotor diameters, i.e., $d' = 10$, for certain operating conditions, it is still necessary to reorient the wake generated by T1. This observation indicates that at a distance of ten rotor diameters from T1, the velocity field has not yet fully recovered. Fourthly, since the number of orange lines decreases as the value of I increases, it is deduced that the lower the turbulent intensity of the wind, the more justified it is to reorient T1 in order to maximize the power gain of T1 and T2. This trend parallels the effect of U' on γ_b, indicating slower recovery of the wake velocity deficit in less turbulent conditions. However, notable exceptions are evident in the fourth column of the plot, where high turbulence does not preclude the benefit of reorienting T1.

Fig. 8 shows partial response plots, which describe how the model's response changes when each predictor varies. Each plot displays the probability that the response, γ_b, takes values of 0 and 1 as the respective predictor varies, while keeping the rest constant at their mean values. The pronounced variations in the curves for $\gamma_b = 1$ in Figs. 8(a) and 8(b) suggest that the predictors y' and U' have a significant impact on the turbines' generated power, directly influencing the model's response. In contrast, Figs. 8(c) and 8(d) display flatter curves for $\gamma_b = 1$ with values lower than those in Figs. 8(a) and 8(b), indicating that the predictors d' and I have a comparatively lesser effect on the model's response when compared to y' and U'.

For illustrative purposes, model M0 was used to predict the geometric locus of coordinates for T2 where T1 should be yawed to optimize the power gain of the turbine pair shown in Fig. 3. Fig. 9(a) presents the results. While T1 is fixed at $(0, 0)$, T2 is placed at $(5D, 0.5D)$. For clarity, T2's coordinates are indicated by black dashed lines. The x-coordinate ranges from 0 to $10D$ and the y-coordinate from $-D$ to D, with 100 points in each direction. The region beyond the model's fitting interval (extrapolation region) is indicated by solid red lines. Redirecting T1 is beneficial when T2's center falls within the yellow region, henceforth termed the *yaw control region*. As depicted in Fig. 9(a), this yellow contour region is relatively narrow, indicating that turbines arranged in a regular line (e.g., along $y = 0$) may not benefit significantly from yaw control. A small shift in wind direction could easily place the turbines outside this effective yaw control region. Conversely, in irregularly arranged wind farms, turbines are more randomly distributed, covering a broader area. This increases the likelihood that at least one turbine will be within the effective yaw control region of another. This implies

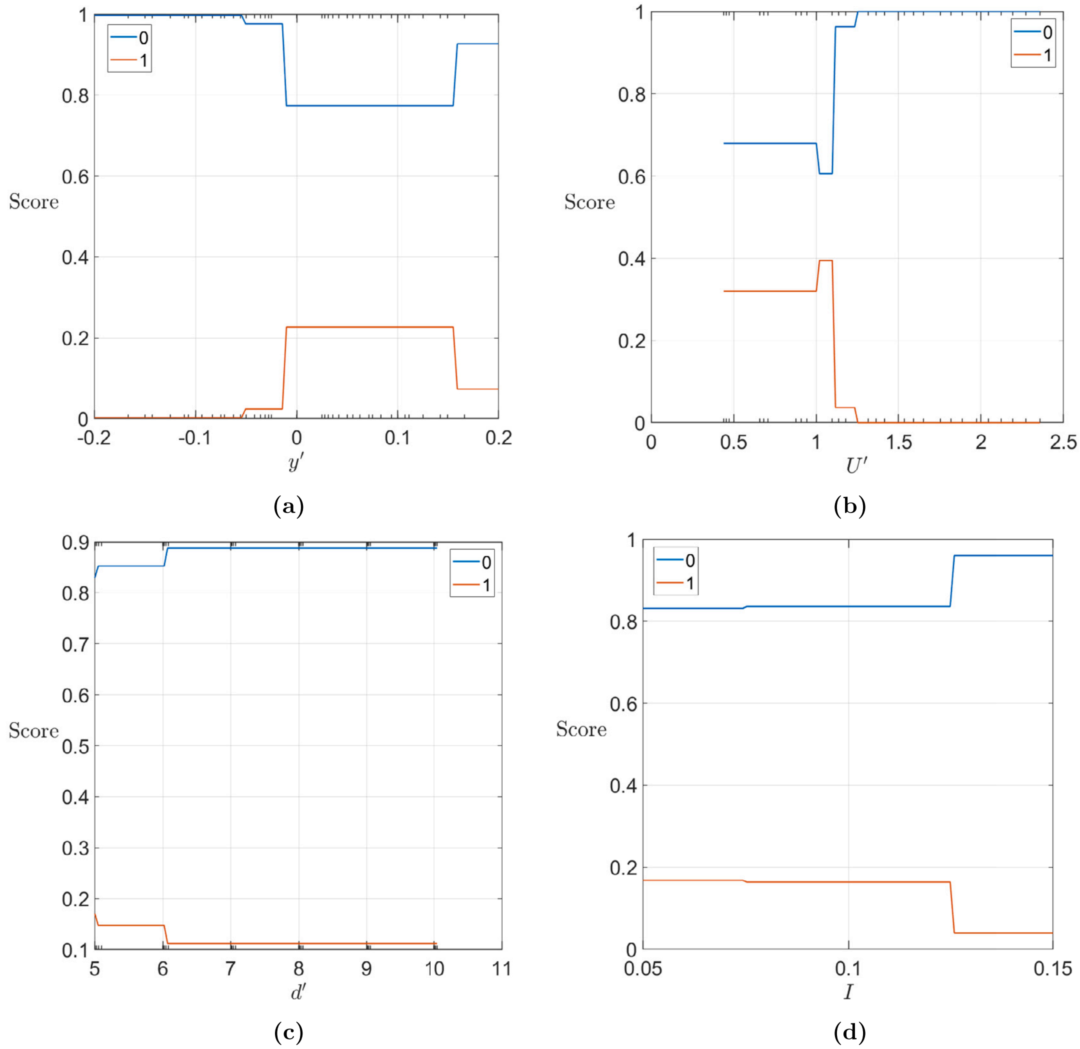

Fig. 8. Partial response plots of the classification model. Scores obtained based on predictors: (a) y', (b) U', (c) d', (d) I.

that yaw control would be significantly more effective in irregularly arranged farms compared to regularly arranged ones. This observation is consistent with the findings of Li et al. (2022), which concluded that yaw control is particularly effective in irregularly arranged wind farms for enhancing power generation, compared to axial induction control.

Fig. 9(b) shows how the locus of points from Fig. 9(a) is affected when wind velocity increases, with the relative wind velocity changing from $U' = 1$ to $U' = 1.2$, making yaw control of T1 no longer beneficial. Similarly, Fig. 9(c) illustrates how the locus of points from Fig. 9(a) is affected when wind turbulence intensity increases from $I = 5\%$ to $I = 15\%$, restricting yaw control of T1 to a very limited region extending from $x = 5D$ to about $x = 6D$ for positive y values.

Since they are expressed in terms of turbine rotor diameter, Figs. 9(a), 9(b), and 9(c) are identical whether the turbine diameter is 126 m, 198 m, 240 m, or any intermediate value. These figures demonstrate that the yaw control region follows a complex pattern, which does not match the turbine wake, as can be confirmed by comparing Figs. 3 and 9(a).

3.2. Regression models for yaw angle and percentage power gain

After performing stepwise regression, the adjusted model for the optimal yaw angle of T1 was obtained, given by Eq. (6):

$$\gamma^* = a_0 + a_1 y' + a_2 d' + a_3 I + a_4 y' d' + a_5 y' I + a_6 (y')^2 \tag{6}$$

Wind speed was found not to significantly affect the yaw angle of T1. Table 6 presents the coefficients of the model obtained in the fit along with their respective p-values. The r^2 and adjusted r^2 of the model were found to be 0.882 and 0.881, respectively, indicating an acceptable goodness of fit. The standard error of the model was 2.20 degrees, based on 536 error degrees of freedom. Unlike previous models that required numerous simulations, the fitted statistical model for the optimal yaw angle involves only evaluating a second-degree polynomial.

Fig. 10 presents the adjusted response plots of M1, which show the effect of each predictor on the optimal yaw angle γ^*. The red dots represent the model's response for each instance in Table 5, while the blue curve fits these responses. The slightly negative responses obtained at the right end of Fig. 10(a) are due to the fitting error of M1.

Figs. 10(a) and 10(b) show that as the distance between T1 and T2 increases, either in the spanwise or streamwise flow direction, γ^* decreases. This trend aligns with findings from Zong and Porté-Agel (2021), indicating that as the spanwise distance between turbines increases, there is a reduced requirement for wake manipulation.

Fig. 10(c) shows that as turbulence intensity increases, γ^* decreases. This is because higher turbulence intensity causes the wake to recover more quickly, leading to a reduction in the optimal yaw angle. This observation aligns with the experimental results of Ozbay et al. (2012), which found that at high turbulence intensity levels, yawing the upstream turbine negatively impacts overall efficiency.

It is important to note that Eq. (6) provides the optimal yaw angle for maximizing the power output of a two-turbine array. However, yaw

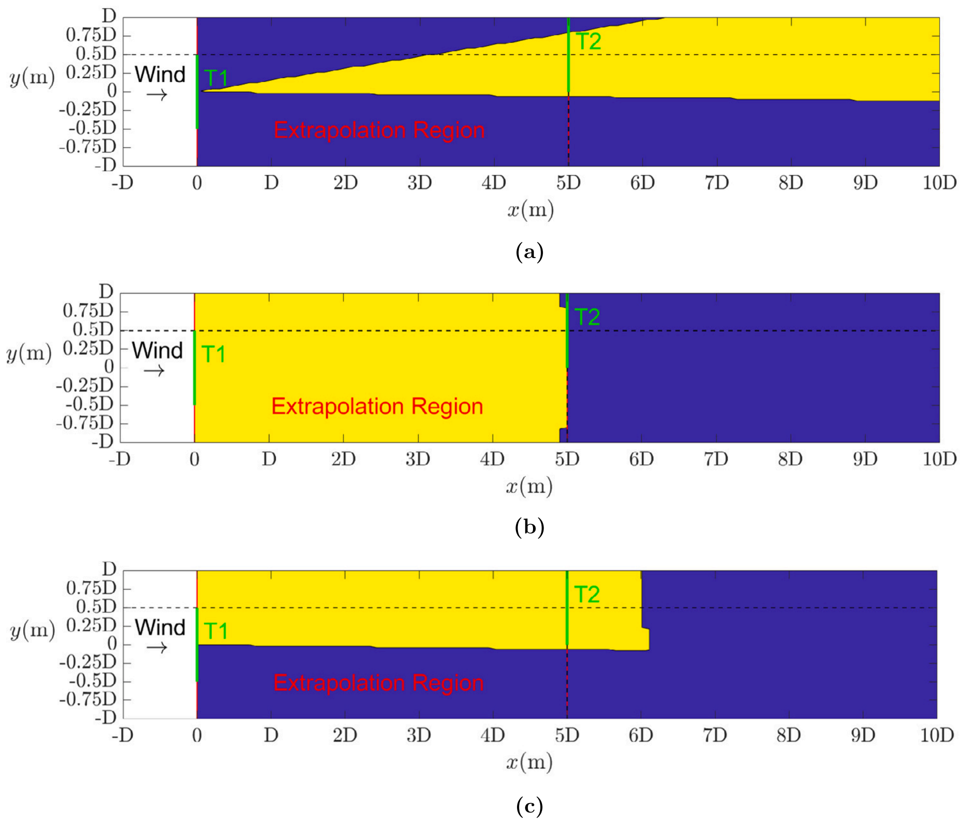

Fig. 9. Contour plot showing the geometric locus for yaw adjustment of T1: (a) same conditions as in Fig. 3, (b) same conditions but with relative velocity changed from $U' = 1$ to $U' = 1.2$, (c) same conditions but with turbulence intensity changed from $I = 5\%$ to $I = 15\%$.

Table 6
Coefficients and associated p-values of adjusted models using predictors in their respective ranges of variation.

M1			M2		
Coefficient	Estimation	p-value	Coefficient	Estimation	p-value
a_0	39.192	2.4864e−184	b_0	127.76	8.6876e−40
a_1	−64.233	9.7978e−07	b_1	391.83	8.0181e−09
a_2	−1.1153	3.3776e−28	b_2	−298.93	6.8437e−26
a_3	−107.25	2.4459e−66	b_3	−3.8111	2.1729e−06
a_4	−9.8687	6.419e−13	b_4	−874.01	1.3355e−20
a_5	502.28	1.8817e−15	b_5	283.77	0.0047455
a_6	−85.095	0.016974	b_6	−49.264	3.6429e−16
			b_7	−7.9737	0.98863
			b_8	7.8223	2.5279e−05
			b_9	843.04	2.145e−15
			b_{10}	17.706	0.0072258
			b_{11}	−5076.6	1.1047e−45
			b_{12}	291.92	2.7198e−21
			b_{13}	2141.5	1.4462e−09
			b_{14}	20.576	4.0673e−05
			b_{15}	−1734.6	3.6748e−12
			b_{16}	314.44	6.7785e−14
			b_{17}	−38.106	7.6463e−07
			b_{18}	1733	1.8346e−20
			b_{19}	43.878	0.049687
			b_{20}	7941.6	1.7406e−15
			b_{21}	−383.75	1.1124e−13
			b_{22}	−3664.5	0.037167
			b_{23}	−3.6036	0.00122
			b_{24}	−1797.9	2.642e−06
			b_{25}	9535.4	6.0563e−45
			b_{26}	−105.37	2.1572e−20

control not only affects power output but also impacts structural loads on the turbines (Annoni et al., 2018; He et al., 2022, 2024). Small yaw angles for the first turbine ($\gamma < 10^{\circ}$) are often inefficient, as they significantly increase fatigue while yielding only marginal power gains (Lin and Porté-Agel, 2020). For example, a yaw angle of -5° was disregarded in He et al. (2022) due to its minimal effect on power generation and negative impact on structural performance. Fig. 4 shows that while no optimal yaw angles were below or equal to 5 degrees, about 14.3% were below or equal to 10 degrees. These smaller angles should be reconsidered to avoid adverse structural loads and extend turbine life, particularly in offshore wind farms, where minimizing maintenance operations is crucial (Boveri and Abb, 2012). Ciri et al. (2018) observed that fatigue loads increase with nonzero misalignment. Additionally, Aju et al. (2023) and Xin et al. (2022) reported that yaw misalignment can affect power output fluctuations.

Model M1 was used to predict the optimal yaw angle for T1 that maximizes power gain for the turbine pair based on T2's coordinates, under the same conditions as those used for Model M0 to predict the yaw control region (Figs. 9(a) and 9(c)). The results are shown in the contour plots of Figs. 11(a) and 11(b). The x-coordinate ranges from $5D$ to $10D$ and the y-coordinate from $-D$ to D, with 100 points in each direction. Comparison of Figs. 11(a) and 11(b) reveals that T1's optimal yaw angle decreases as wind turbulence intensity increases from $I = 5\%$ to $I = 15\%$. This trend is consistent with the decrease in γ^* with higher I values shown in Fig. 10(c).

Following the same fitting procedure used for determining γ^*, the percentage power gain of the wind turbine pair achieved through active yaw control was adjusted. This process resulted in the fitted model represented by Eq. (7):

$$\begin{aligned}\Delta P = {} & b_0 + b_1 y' + b_2 U' + b_3 d' + b_4 I + b_5 y' U' + b_6 y' d' + b_7 y' I \\ & + b_8 U' d' + b_9 U' I \\ & + b_{10} d' I + b_{11} (y')^2 + b_{12} (U')^2 + b_{13} (I)^2 + b_{14} y' U' d' \\ & + b_{15} y' U' I + b_{16} y' d' I \\ & + b_{17} U' d' I + b_{18} (y')^2 U' + b_{19} (y')^2 d' + b_{20} (y')^2 I\end{aligned}$$

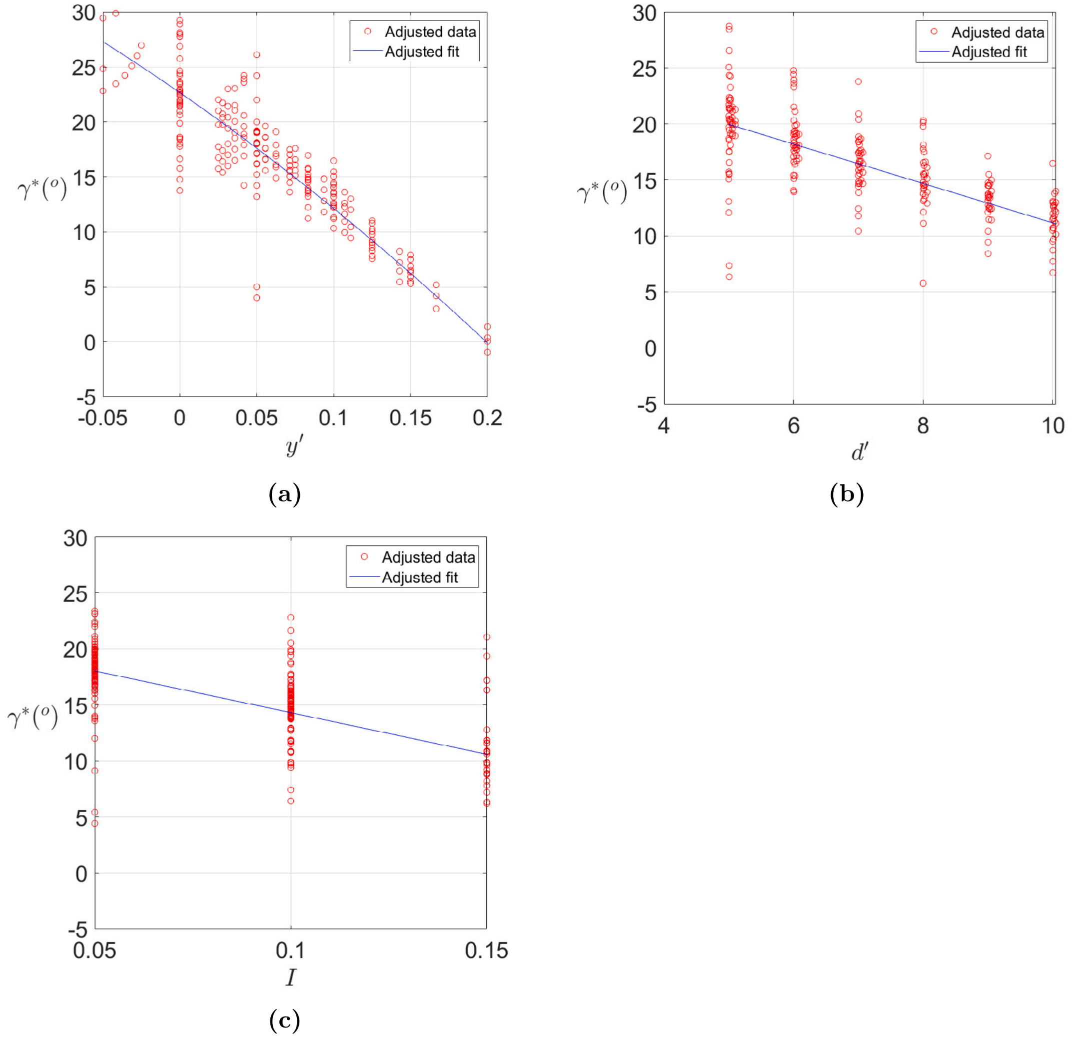

Fig. 10. Adjusted response plots for the optimal yaw angle of T1, with predictors: (a) y', (b) d', (c) I.

$$+ b_{21}y'(U')^2 + b_{22}y'(I)^2$$
$$+ b_{23}(U')^2d' + b_{24}U'(I)^2 + b_{25}(y')^3 + b_{26}(U')^3 \quad (7)$$

Since not only the four predictors but also some interaction, quadratic and cubic terms turned out to be significant, it is inferred that the relationship between ΔP and the predictors is more complex than that presented by γ^* in Eq. (6). The highly nonlinear relationship between the response ΔP and the predictors suggests that a more accurate prediction of this response would require the inclusion of higher-order terms in M2. Table 6 presents the coefficients of the model obtained in the fit along with their respective p-values. The r^2 and adjusted r^2 of the model were found to be 0.912 and 0.908, respectively, indicating an acceptable goodness of fit. The standard error of the model was 1.53%, based on 516 error degrees of freedom.

Fig. 12 shows the adjusted response plots of M2, which illustrate the effect of each predictor on ΔP. Figs. 12(a), 12(b), 12(c), and 12(d) generally demonstrate that increasing the distance between T1 and T2 in either the spanwise or streamwise wind direction, as well as higher wind speeds and/or turbulence intensity, result in lower power gains when applying AYC. The slightly negative responses obtained in Figs. 12(a), 12(b), and 12(d) are due to the fitting error of M2. Overall, the trends observed in Fig. 12 align well with results obtained by other researchers and with the classification model results shown in Fig. 7.

Fig. 12(a) demonstrates that the highest power gain occurs when the spanwise distance between T1 and T2 is approximately 4% of their streamwise distance ($y' \approx 0.04$). This observation is consistent with findings from studies such as Zong and Porté-Agel (2021), which explored power enhancement in a three-turbine wind farm and found that the maximum improvement through AYC occurs at $y' = 0.07$. This effect is attributed to mitigating power losses in the wake center, where yaw control during partial wake conditions enables downstream turbines to avoid high-power-loss areas. Specifically, Fig. 12(a) indicates that the maximum power gain under partial wake conditions ($y' = 0.04$) is approximately 8.7%, higher than the 5.5% gain under full wake conditions ($y' = 0$), highlighting the reduced effectiveness of AYC in fully-waked conditions.

Consistent with the trends depicted in Figs. 12(b) and 12(d), Wei et al. (2023) found that AYC is more effective in conditions with lower incoming wind speeds and reduced turbulence intensity.

Moreover, the effectiveness of yaw control diminishes as turbine spacing increases, as illustrated in Fig. 12(c). This observation is reinforced by He et al. (2024), who demonstrated that closer turbine spacing significantly enhances power production due to intensified wake effects. Similar findings were reported by Zong and Porté-Agel (2021) and Bastankhah and Porté-Agel (2019), highlighting reduced effectiveness of yaw angle control with greater streamwise turbine spacing. Additionally, Wei et al. (2023) noted significant variations in the efficiency of AYC based on turbine spacing.

Additionally, since rotor diameter appears in the denominator of parameter d', Fig. 12(c) shows that larger rotor diameters lead to greater

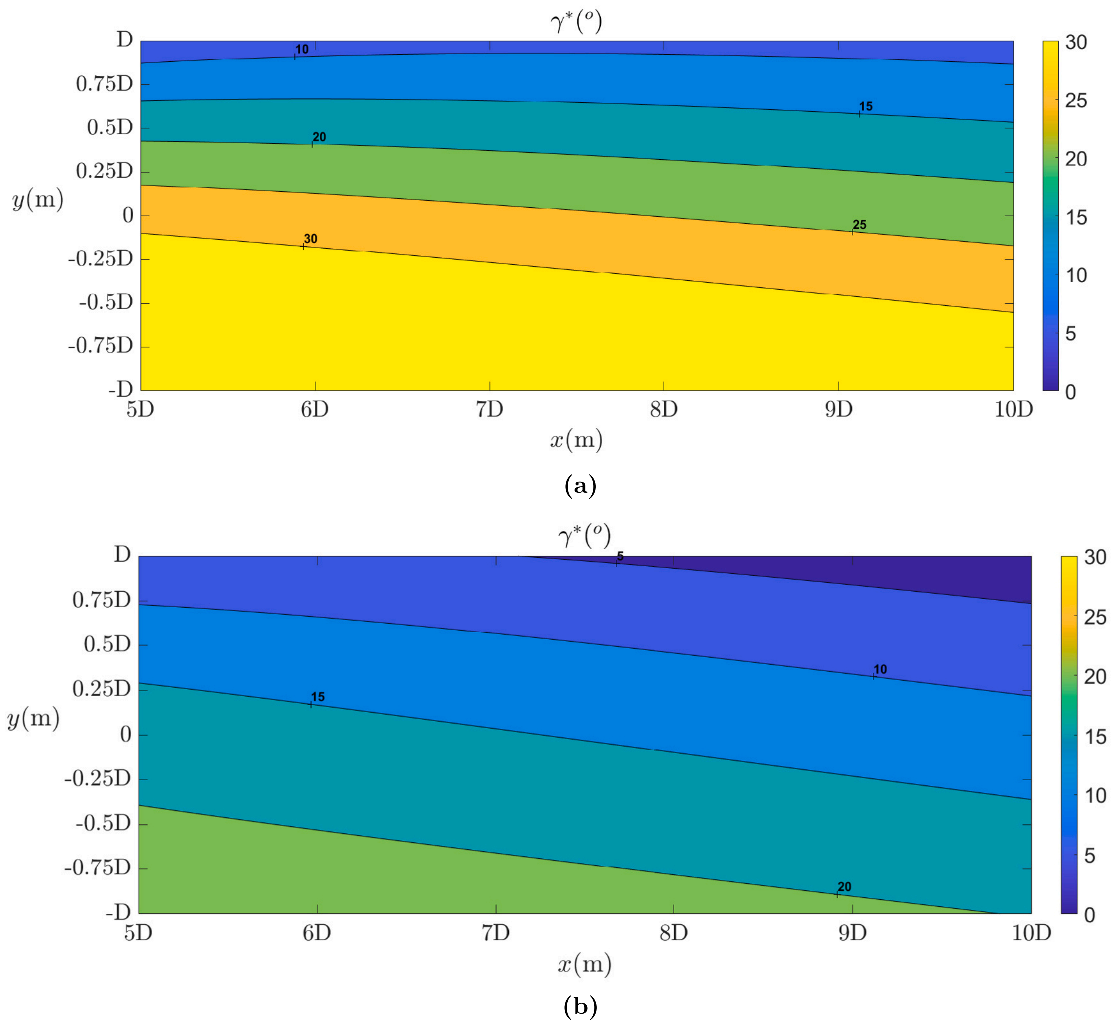

Fig. 11. Contour plot showing T1's optimal yaw angle as a function of T2's coordinates: (a) same conditions as in Fig. 3, (b) same conditions but with turbulence intensity changed from $I = 5\%$ to $I = 15\%$.

power gains from AYC. This finding is consistent with the findings of Ciri et al. (2018), who used LES to assess yaw control in a three-turbine cascade with varying turbine sizes. Their study concluded that larger rotor diameters induce more significant wake deflection, thereby achieving higher power improvements. They explain that large turbines produce vortical structures with slow dynamics, causing the wake to maintain the initial orientation induced by yaw misalignment. In contrast, smaller turbines generate vortices that dissipate more quickly, leading to a rapid realignment of the wake with the free stream. This weaker lateral displacement of the wake results in a greater impact on downstream turbines. Hence, the yaw control strategy should account for turbine spacing and size, where a dense array of large wind turbines (low d') enables more efficient control than a sparse array of small wind turbines (large d'). The tendency for reduced power gains with increasing turbine distance was similarly observed by Kumar et al. (2023), who conducted wind tunnel experiments on a 3×3 turbine array. Applying extremum seeking control algorithms for yaw optimization, they tested two layouts: aligned ($d' = 5$) and staggered ($d' \approx 5.4$). While the aligned configuration resulted in a power gain of up to 5.8%, the staggered layout yielded a lower gain of around 2%.

Fig. 12(d) illustrates that when hub-height turbulence levels reach 15%, active yawing does not improve power output. This observation is consistent with the findings of Zong and Porté-Agel (2021), who suggest that active yaw control is more effective in low-turbulence environments. Similarly, He et al. (2024) observed that power enhancement can reach up to 18% at low turbulence levels, while higher turbulence levels reduce power gains. Additionally, Bastankhah and Porté-Agel (2019) noted that under highly turbulent inflow conditions, opportunities for wake mitigation strategies to enhance downstream turbine performance are limited.

Model M2 was used to predict the percentage power gain of the turbine pair based on the optimal yaw angle of T1, under the conditions shown in Fig. 11. The results are displayed in Fig. 13. To ensure validity, colorbar limits were set between 0% and 12% to exclude negative power gains. Comparison of Figs. 13(a) and 13(b) shows that the region of high power gain decreases as wind turbulence intensity increases from 5% to 15%, consistent with the trend observed in Fig. 12(d). Additionally, the high power gain regions in Figs. 13(a) and 13(b) correspond to the yaw control regions (yellow areas) in Figs. 9(a) and 9(c). The first region extends broadly in the x direction, covering a wide range of intermediate y values, while the second region is confined to a narrower range of x values, predominantly covering positive y values.

Each point in Figs. 11 and 13 represents a simulation of the wind velocity field and optimization of the yaw angle. These contour maps, generated using surrogate models M0, M1, and M2, offer valuable insights for selecting optimal yaw control strategies for offshore turbines in low-to-moderate wind speeds and turbulence intensity. As with Fig. 9, Figs. 11 and 13 are scale-independent, as they are presented in terms of turbine rotor diameter.

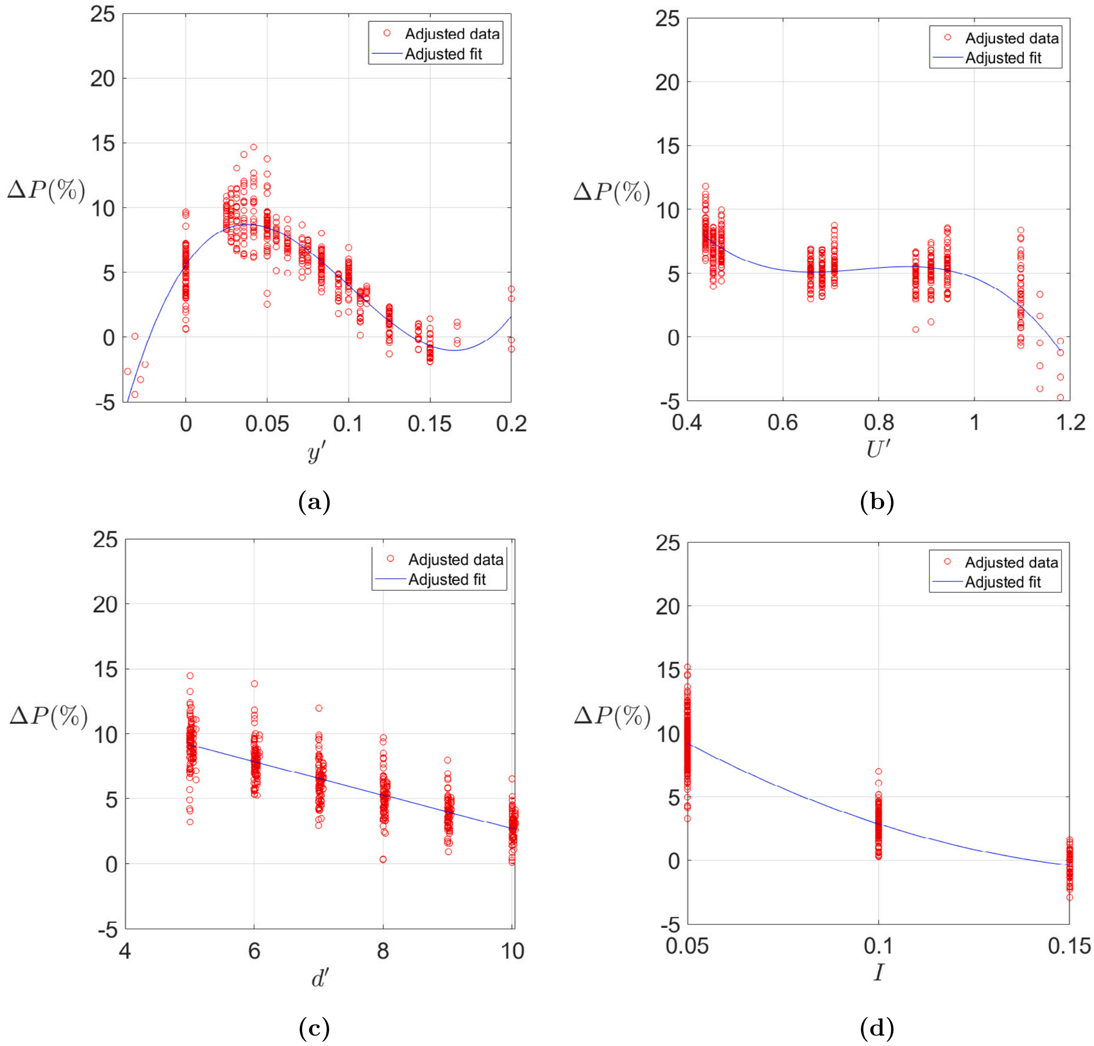

Fig. 12. Adjusted response plots for the percentage power gain of T1 and T2, with predictors: (a) y', (b) U', (c) d', (d) I.

3.3. Sensitivity analysis

To gain a deeper quantitative understanding of the dependency of the optimal yaw angle and percentage power gain on the predictors, the Relative Importance Index (RII) was calculated with the predictors assuming values within the variation intervals for which the responses are positive, as identified in Figs. 10 and 12. For Model M1, based on Fig. 10, the variation intervals for the predictors are: $-0.05 < y' < 0.2$, $5 < d' < 10$, and $0.05 < I < 0.15$. For Model M2, based on Fig. 12, the variation intervals for the predictors are: $-0.02 < y' < 0.14$, $0.44 < U' < 1.15$, $5 < d' < 10$, and $0.05 < I < 0.14$.

A method similar to that described in Sadan et al. (2016) was followed to calculate the RII. This index quantifies the relative impact of each input parameter on the response, normalized by the total impact of all parameters. All terms in Models M1 and M2 are included in this calculation. For example, the RII for the input parameters of Model M1 is computed as follows:

$$\mathrm{RII}_{y',1} = \frac{\Delta\gamma^*_{y'}}{\Delta\gamma^*_{\mathrm{tot}}}, \quad \mathrm{RII}_{d',1} = \frac{\Delta\gamma^*_{d'}}{\Delta\gamma^*_{\mathrm{tot}}}, \quad \mathrm{RII}_{I,1} = \frac{\Delta\gamma^*_{I}}{\Delta\gamma^*_{\mathrm{tot}}}$$

where $\Delta\gamma^*_{\mathrm{tot}} = \Delta\gamma^*_{y'} + \Delta\gamma^*_{d'} + \Delta\gamma^*_{I}$ represents the total impact of the three predictors on γ^*. Here, $\mathrm{RII}'_{y}, 1$ denotes the RII for predictor y' calculated using Model M1, with $\Delta\gamma^*_{y'}$ representing the absolute maximum change in γ^* due to variations in y'. For Model M2, which includes four parameters (y', U', d', and I), a similar RII calculation can be performed.

Fig. 14 illustrates the RII for each predictor included in both M1 and M2. For M1, it is observed that the effect of y' is the most significant, followed by d', and then I. For M2, the results reveal that the effect of I on the response is the most important, followed by y', then U', and finally d'. This observation aligns with the experimental study reported in Ozbay et al. (2012), which examined the power output of two turbines in tandem and found that overall efficiency strongly depends on the incoming flow turbulence intensity level. While the predictors have a comparable relative importance on the response of model M2, the predictor y' is significantly more relevant to the response of model M1 than the other predictors.

Although the RII does not account for the direction of change in optimal yaw angle and power percentage gain, Figs. 10 and 12 illustrate that increasing y', U', d', and I generally leads to a decrease in both the optimal yaw angle and the power percentage gain. This suggests that careful consideration of farm layout, wind conditions, and turbine characteristics is essential for selecting the most effective yaw control strategy. Specifically, yaw control is found to be more beneficial in dense wind farms with lower d' and y' values compared to sparse wind farms, particularly under mild wind conditions.

3.4. Models evaluation

Three case studies were conducted to evaluate the performance of the classification and regression models under different layouts. In

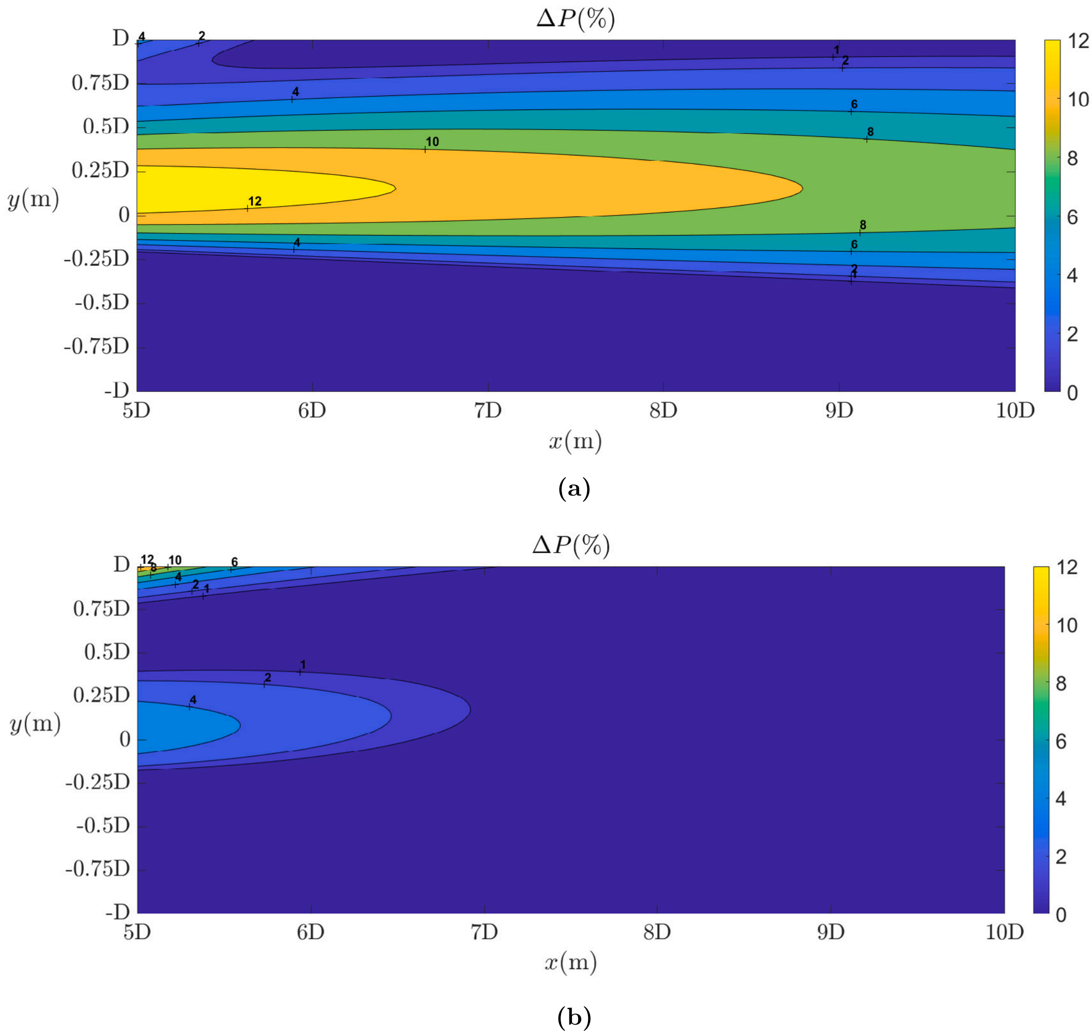

Fig. 13. Contour plot showing the percentage power gain of the turbine pair for T1's optimal yaw angle as a function of T2's coordinates: (a) same conditions as in Fig. 3, (b) same conditions but with turbulence intensity changed from $I = 5\%$ to $I = 15\%$.

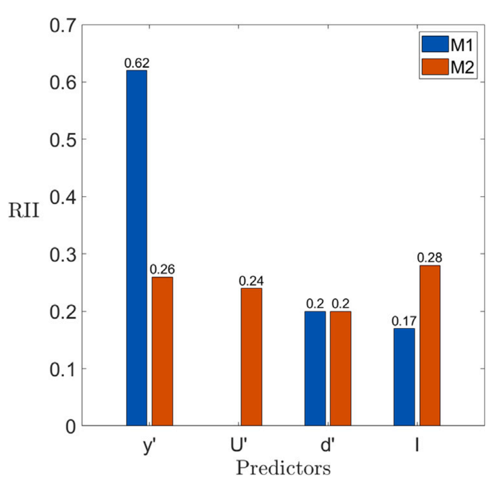

Fig. 14. Predictor relative importance index grouped by model.

the first case (Case 1), the spanwise distance between T1 and T2 (y) was varied while keeping the streamwise distance (x) constant. In the second case (Case 2), the streamwise distance (x) was varied while keeping the spanwise distance (y) constant. In the third case (Case 3), a comparative validation was conducted against results from another study using the Horns Rev I wind farm configuration. These scenarios ensure that the models are tested under both full-wake and partial-wake conditions. The results and their implications are discussed below.

3.4.1. *Case 1: Constant* **x**, *variable* **y**

In Case 1, the following parameters related to wind conditions and turbine scale were set: $I = 5\%$, $U = 11$ m/s, $U_r = 11$ m/s, and $D = 198$ m, with the latter two corresponding to the IEA 10 MW turbine. Table 7 presents the values for the predictors in this case.

The first case for comparing the fitted models with simulation results involved varying y from $-0.25D$ to D in steps of $0.25D$, while keeping x constant at $5D$. This setup ensured a significant aerodynamic interaction between T1 and T2 due to the relatively short distance. Fig. 15 displays the contour plot showing the geometric locus for yaw adjustment of T1 for Cases 1 (a) and (d) as examples. T2's center is marked with a red dot for each of the six runs (a)–(f). The optimal yaw angle γ^*, calculated using regression model M1 and rounded to the nearest integer, was used in these examples.

After running the six simulations corresponding to Case 1, the results shown in Table 7 were obtained, presented alongside those obtained using models M0, M1, and M2. The classification model correctly classified all six simulations, with the first and last ones resulting in $\Delta P < 1\%$, classified with a $\gamma_b = 0$ response, and the remaining four with $\Delta P > 1\%$, classified with a $\gamma_b = 1$ response. Since

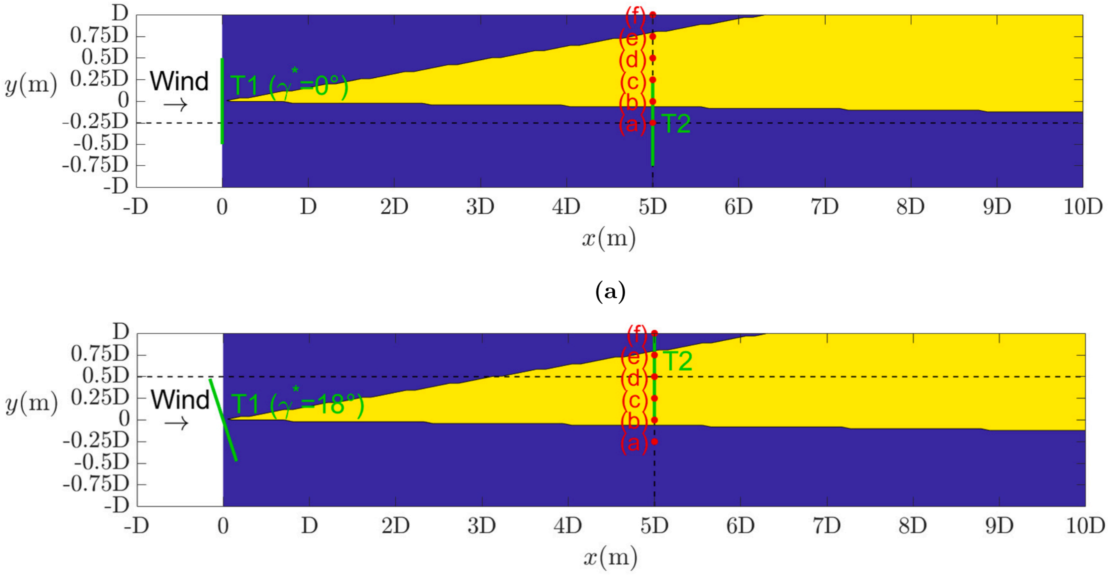

(a)

(b)

Fig. 15. Contour plot showing the geometric locus for yaw adjustment of T1: (a) Case 1, run (a); (b) Case 1, run (d).

Table 7
Results obtained with the models and simulations in Case 1.

	Predictors				Simulations		M0	M1	M2
	y'	U'	d'	I [%]	γ^* [°]	ΔP [%]	γ_b	γ^* [°]	ΔP [%]
(*a*)	−0.0500	1	5.0062	5	0	0	0	0	0
(*b*)	0.0000	1	5.0000	5	17	8.46	1	28.25	11.63
(*c*)	0.0500	1	5.0062	5	21	15.77	1	23.60	12.53
(*d*)	0.1000	1	5.0249	5	17	12.66	1	18.50	6.93
(*e*)	0.1500	1	5.0559	5	14	5.78	1	12.92	1.97
(*f*)	0.2000	1	5.0990	5	13	9.88×10^{-6}	0	0	0

Table 8
Results obtained with the models and simulations in Case 2.

	Predictors				Simulations		M0	M1	M2
	y'	U'	d'	I [%]	γ^* [°]	ΔP [%]	γ_b	γ^* [°]	ΔP [%]
(*a*)	0.0500	1	5.0062	5	21	15.77	1	23.60	12.53
(*b*)	0.0417	1	6.0052	5	21	17.71	1	22.88	11.95
(*c*)	0.0357	1	7.0045	5	20	16.93	1	22.04	11.21
(*d*)	0.0312	1	8.0039	5	20	15.85	1	21.12	10.41
(*e*)	0.0278	1	9.0035	5	19	14.71	1	20.16	9.60
(*f*)	0.0250	1	10.0031	5	18	13.55	1	19.17	8.79

the first and last simulations were classified with a $\gamma_b = 0$ response by M0, the corresponding predictions for M1 and M2 were not calculated. Therefore, in those cases, no active yaw control was applied, and $\gamma^* = 0^o$ and $\Delta P = 0\%$ were assumed without quantifying the associated errors. The average computation times for models M0, M1, and M2 to calculate γ_b, γ^*, and ΔP across the six instances in Case 1 were approximately 0.8594 s, indicating that each simulation run completed within tenths of a second.

Fig. 16 presents the percentage relative errors associated with the γ^* and ΔP responses obtained with M1 and M2, symbolized by ϵ_{γ^*} and $\epsilon_{\Delta P}$, respectively. Except for the second instance, ϵ_{γ^*} was lower than $\epsilon_{\Delta P}$, resulting in average errors of 23.78% and 42.27%, respectively. Furthermore, ϵ_{γ^*} decreases as turbine spacing increases, while the opposite occurs with $\epsilon_{\Delta P}$.

3.4.2. Case 2: Constant *y*, variable *x*

In Case 2, the wind conditions and turbine scale were identical to Case 1. Table 8 shows the predictor values. The second case for comparing the fitted models with simulation results involved varying x from $5D$ to $10D$ in steps of D, while keeping y constant at $0.25D$. This constant spanwise distance for turbine T2 ensured partial wake interference between the turbines. Fig. 17 shows the contour plot of the geometric locus for yaw adjustment of T1 for Cases 2 (a) and (d), selected as examples. In these cases, the optimal yaw angle γ^*, computed using regression model M1 and rounded to the nearest integer, was utilized.

After running the six simulations for Case 2, the results obtained are shown in Table 8, alongside those from models M0, M1, and M2. Model M0 correctly classified all six cases, assigning a $\gamma_b = 1$ response, consistent with achieving $\Delta P > 1\%$ in all six simulations. This outcome was expected, as Fig. 7 indicates that for the Case 2 conditions ($0.025 < y' < 0.05$, $U' = 1$, $5.0062 < d' < 10.0031$, and $I = 0.05$), the estimated response by M0 would likely be $\gamma_b = 1$. The time required by models M0, M1, and M2 to calculate γ_b, γ^*, and ΔP for the six instances in Case 2 was approximately 0.1003 s.

Fig. 18 presents the percentage relative errors for the γ^* and ΔP responses obtained with models M1 and M2. Generally, ϵ_{γ^*} was lower than $\epsilon_{\Delta P}$, with average errors of 8.32% and 31.81%, respectively. Similar to Case 1, ϵ_{γ^*} tends to decrease as turbine spacing increases, while $\epsilon_{\Delta P}$ shows the opposite trend.

In summary, for Cases 1 and 2, the average errors were $\epsilon_{\gamma^*} = 14.50\%$ and $\epsilon_{\Delta P} = 37.04\%$. Model M1 showed relatively accurate results, with precision generally improving as the distance between T1 and T2 increased, except for Case 1(b), where T2 was very close to T1 (at $x = 5D$ and $y = 0$, with $d' = 5$). Experimental data obtained by other authors (Kumar et al., 2023) suggest that the optimal yaw angle of the upstream wind turbine in Case 1(b) is approximately 28 degrees for a layout with $d' = 5$ and $y' = 0$. This value aligns more closely with the predictions of Model M1 than with those obtained from FLORIS. One possible reason for the large error is that in the near wake region, the FLORIS GCH model employs a different approach to model the velocity field compared to the far wake region, which uses a Gaussian velocity profile. Specifically, it assumes a linearly converging cone-shaped velocity profile, with its base at the rotor and tip at the near wake region's end (beginning of the far wake region) (van Beek

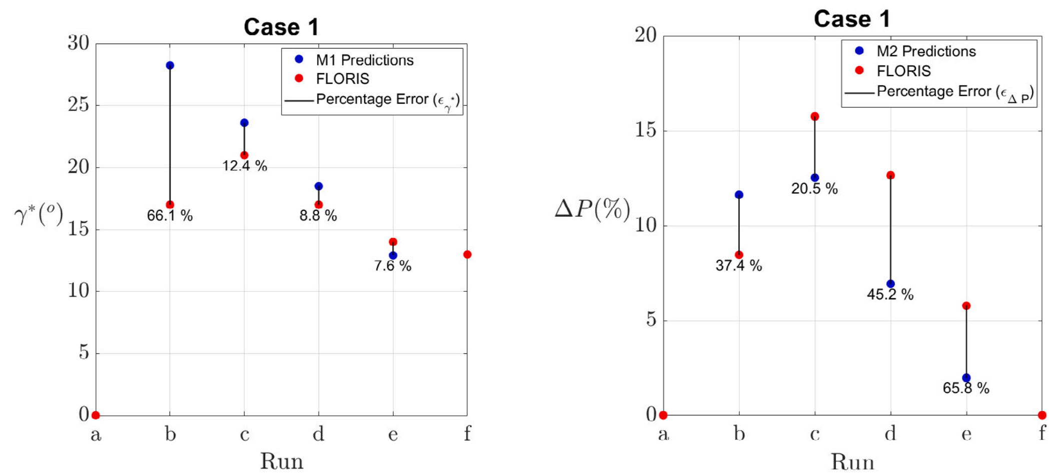

(a) (b)

Fig. 16. Comparison of model predictions and simulation results for Case 1: (a) Optimal yaw angle, (b) Percentage power gain.

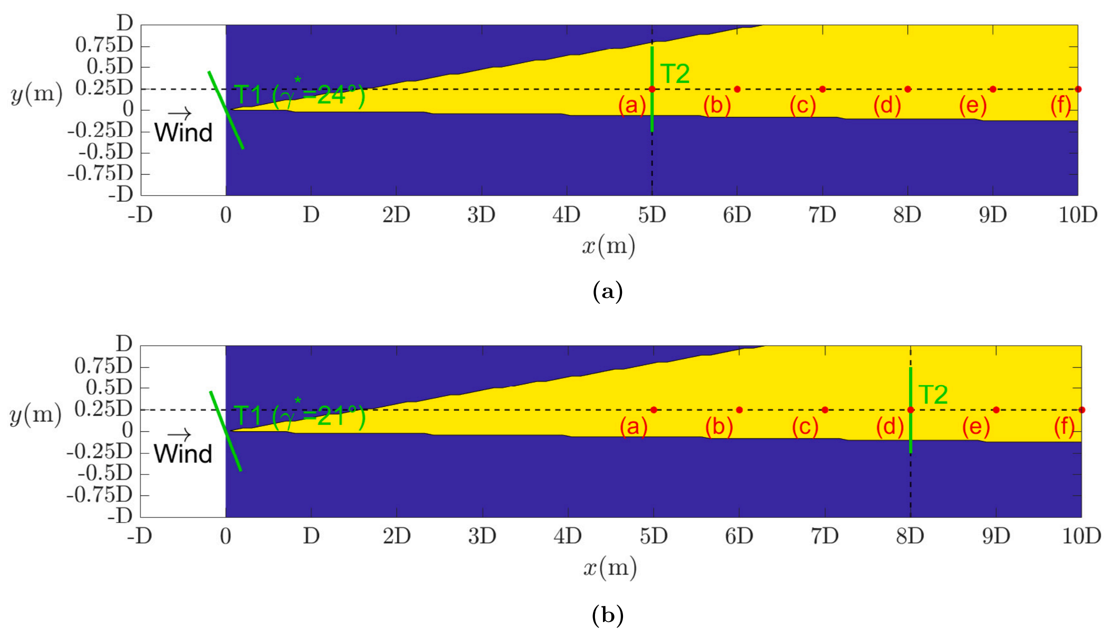

Fig. 17. Contour plot showing the geometric locus for yaw adjustment of T1: (a) Case 2, run (a); (b) Case 2, run (d).

et al., 2021). This discrepancy can lead to difficulties for the regression model in fitting FLORIS data near the boundary between the near and far wake regions, as differing models are used to compute velocity, directly impacting turbine-generated power and optimal yaw angle. Excluding this case, M1's average error was 8.7% for $d' \geq 5.0062$. While M2 achieved an acceptable r^2 and followed simulation trends, its high errors indicate it is better suited for qualitative analysis rather than precise predictions, likely due to the nonlinear nature of power gain compared to the optimal yaw angle. Overall, M1 tends to overestimate the yaw angle, whereas M2 underestimates the power gain compared to simulation results.

To assess the computational efficiency of the models, the time required by M0, M1, and M2 to calculate γ_b, γ^*, and ΔP across 4374 instances was measured, totaling approximately 15.1296 s. This rapid computation is a key advantage, as the models only require evaluating a decision tree and two polynomials, bypassing costly numerical simulations. This efficiency allows for quick predictions of the optimal yaw angle and turbine redirection without specialized software, making the technique accessible even in a spreadsheet.

While FLORIS can quickly calculate velocity fields and power output, its optimization algorithms require multiple iterations to determine an optimal yaw configuration, often involving hundreds of simulations, especially in large wind farms. Each shift in conditions necessitates a fresh set of simulations and optimization. In contrast, the statistical model, developed using a two-turbine setup, scales readily to varied farm configurations and allows for the exclusion of turbines under maintenance. By focusing optimization on each turbine individually, the model adapts efficiently to local condition changes. Additionally, the polynomial regression formulas derived from FLORIS data are straightforward to implement in widely available software, making them practical for integration into workflows and computational systems such as Supervisory Control and Data Acquisition (SCADA) software.

To assess the computational efficiency of model M1 relative to established yaw optimization methods, the Serial-Refine (SR) method was applied to calculate the optimal yaw angles for turbine T1 across all simulations in Case 1 and Case 2. Additionally, the SLSQP algorithm was tested, but it required significantly more computation time than

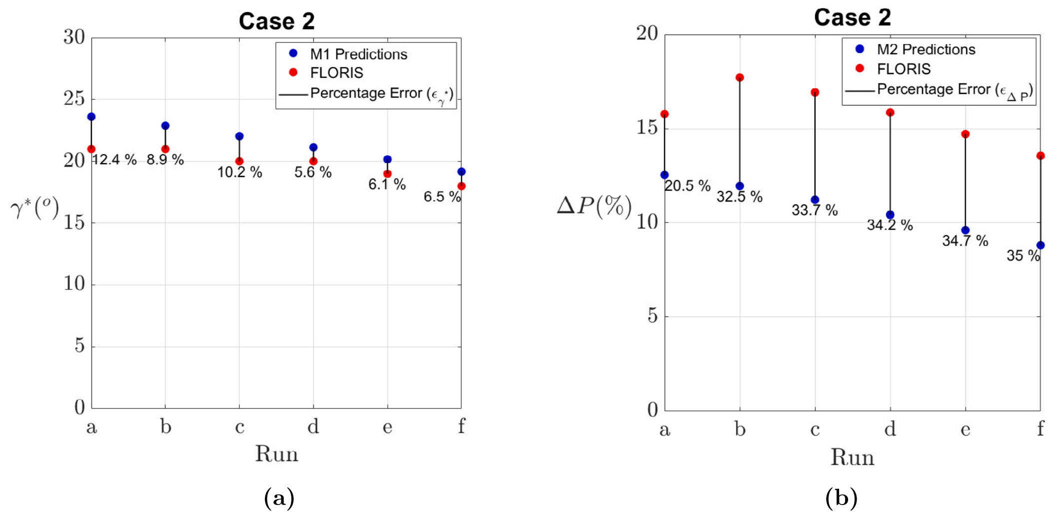

Fig. 18. Comparison of model predictions and simulation results for Case 2: (a) Optimal yaw angle, (b) Percentage power gain.

both the SR and M1 methods. Previous studies have demonstrated that the SR method achieves computational times up to 10 times faster than the SLSQP optimizer (Fleming et al., 2022).

Although both SR and M1 aim to optimize yaw angles, their computational approaches are fundamentally different. Model M1, represented by the polynomial regression equation in Eq. (6), directly estimates the optimal yaw angle for turbine T1. The implementation of M1 is encapsulated in the function `YawFitted`, which follows a three-step process: first, it computes farm power under a baseline scenario with zero yaw angles; next, it applies M1 to determine the optimal yaw angle; and finally, it recalculates farm power with the optimized yaw angle to determine the percentage power gain. These steps are detailed in the pseudocode shown in Fig. 19, where comments and keywords are color-coded for clarity.

The SR method, in contrast, uses a two-step process. The initial "Serial" pass sequentially tests five yaw angles within the range [0, 30] degrees for each turbine, starting upstream and proceeding downstream. The subsequent "Refine" pass evaluates five additional angles near the optimal yaw angle identified during the Serial pass. The pseudocode for the SR method is available in Fleming et al. (2022). For comparison, Fig. 20 summarizes the procedures used to optimize yaw angles with each method.

Figs. 21(a) and 21(b) present the optimal yaw angles derived from both M1 and SR for Cases 1 and 2, as well as the computational time ratios between the methods. In Fig. 21(b), t_{M1} and t_{SR} represent the computational times recorded for model M1 and the SR method, respectively. In Fig. 21(a), the optimal yaw angles from both methods exhibit a similar trend, with the largest deviation observed in run (b) of Case 1, where discrepancies with FLORIS simulation results were previously noted. Fig. 21(b) underscores the computational efficiency of M1, showing that the SR method requires approximately 5 times more computation time than M1, with variations between 4 and 6 times. This disparity arises from the numerous power simulations required for both the Serial and Refine passes in SR, whereas M1 avoids these intensive simulations by providing a direct, approximate yaw angle estimation.

3.5. Case 3: Comparative validation with Horns Rev I wind farm configuration

In Case 3, the developed optimal yaw control model was validated using a single row of ten turbines, replicating the setup analyzed in Bempedelis et al. (2023) for the Horns Rev I wind farm. While their study employed Vestas V80 2 MW turbines, this analysis uses NREL 5 MW turbines, the smallest scale considered in the model fitting. Despite the difference in turbine size, the turbine spacing was maintained at $7D$, consistent with the Horns Rev I wind farm, thus preserving the dimensionless spacing (d'). Wind conditions were aligned with those reported in Bempedelis et al. (2023), specifically with an easterly wind direction (270°) parallel to the turbine row. The free stream turbulence intensity was set at 8%, and the wind speed was adjusted to 5.63 m/s to ensure consistency with the dimensionless velocity value of $U' = U/U_r = 7.9/16 \approx 0.49$ as utilized in the referenced study.

While using free-stream wind velocity and turbulence intensity would offer a preliminary estimate of the optimal yaw angle for all turbines, for greater accuracy, it is essential to consider local turbine wind speeds and turbulence intensities, denoted by the subscript 'ind', as these parameters vary with yaw angle. In this study, local wind velocity and turbulence intensity will be derived from simulations. In practical applications, wind velocity is typically measured with anemometers located at the turbine nacelle. However, since turbulence intensity is not usually measured directly at the nacelle, it can be estimated using historical data. To achieve this, model M1 was applied sequentially for each turbine in the array. Initially, all yaw angles were set to 0°, and the process began by simulating the wind velocity field and yawing the most upstream turbine to maximize power gain. The wind velocity field was then recalculated, and the optimal yaw angle for the second turbine was determined and applied. This process was repeated for each subsequent turbine, with the wind velocity field recalculated each time. Under these conditions, defined by $y' = 0$, $0.424 \leq U' \leq 0.492$, $d' = 7$, and $0.0935 \leq I \leq 0.183$ for all turbines, model M0 indicated that yawing all turbines would enhance power gain. Consequently, all turbines except the last one were adjusted to their optimal yaw angles. Figs. 22(a) and 22(b) present the wind velocity and turbulence intensity for each turbine in the array, where turbine 1 is the most upstream turbine and turbine 10 is the most downstream one. For completeness, the figure also includes the values corresponding to the unyawed scenario. Figs. 23(a) and 23(b) depict the simulated velocity fields at turbine hub height for both the unyawed and yawed scenarios. The yaw angle for each turbine is indicated above the corresponding turbine in the figures. For detailed analysis, optimal yaw angles are presented with two decimal places. However, in practice, wind turbine yaw systems typically control the angle with an accuracy of approximately one degree (Pei et al., 2018).

The simplified optimization procedure described earlier, which uses model M1, assumes that the wind direction realigns with the inflow direction before reaching each turbine. For greater accuracy, a more detailed calculation should account for the local wind direction at each turbine nacelle—typically measured with wind vanes on-site—and adjust the turbine yaw angle based on this local direction. To incorporate

```
FUNCTION YawFitted(fi, j, y, U, d, I)

% Input parameters:
% fi: FLORIS interface object.
% j: Index for storing results.
% y, U, d, I: Dimensionless input parameters for model M1.

% Output:
% yaw_max: Optimal yaw angle for turbine T1.
% DP_max: Percentage power gain compared to the baseline case.

1. Initialize:
- Set the initial yaw angles of turbines T1 and T2 to zero.

2. Baseline case:
- Simulate the wake with yaw angles of T1 = 0 and T2 = 0.
- Compute and store the baseline farm power, P_baseline.

3. Active yaw control case:
- Compute the optimal yaw angle for T1 using model M1:

yaw_max = 39.192 - 1.1153d - 107.25I + y(-64.233 - 9.8687d +
    502.28I - 85.095y)

- Set yaw angles: yaw_max for T1 and 0 for T2.
- Simulate the wake with the updated yaw angles.
- Compute and store the farm power, P_yaw.

4. Compare cases:
- Calculate the percentage power gain:

DP_max = 100 * (P_yaw - P_baseline) / P_baseline

RETURN (yaw_max, DP_max)
```

Fig. 19. Pseudocode for the function YawFitted implementing model M1.

a change in wind direction, the downstream turbine coordinates (x and y) should be modified using a rotation matrix that accounts for the angle difference between the new wind direction and east, and then provided to the model.

For comparative purposes, the results of this study were evaluated against those reported in Bempedelis et al. (2023). In that study, two frameworks were used for calculating optimal yaw angles and turbine efficiency: high-fidelity simulations with Bayesian Optimization (LES-BO) and a FLORIS-based method using the GCH model with the SLSQP optimization algorithm. For turbine efficiency, they used both the LES-BO framework and a multi-fidelity approach combining a low-fidelity model with LES (LF/LES). They reported turbine efficiencies $\eta = \sum_{i=1}^{N} P_i(\gamma = \gamma^*)/\sum_{i=1}^{N} P_i(\gamma = 0°)$ of $\eta = 1.28$ for LES-BO and $\eta = 1.24$ for LF/LES, whereas this study obtained $\eta = 1.22$ using FLORIS. This 22% value represents an average turbine efficiency, indicating that individual turbines within the array may perform either above or below this average.

Fig. 24(a) compares the optimal yaw angles obtained using model M1 with those reported in Bempedelis et al. (2023) using FLORIS. The yaw angles predicted by model M1 exhibit greater consistency across turbines compared to the variations reported in Bempedelis et al. (2023), a favorable characteristic of model M1 as it helps avoid small γ angles that could increase wind loads and negatively affect turbine performance. The trend of decreasing optimal yaw angles in the direction of the wind is driven by the increased turbulence intensity resulting from turbine interactions, as shown in Fig. 22(b), which aligns with the results presented in Fig. 10(c). However, turbulence intensity has the least relative importance in model M1, as shown in Fig. 14, implying that turbines evenly distributed across the wind farm will exhibit similar y' and d' values, leading to similar optimal yaw angles predicted by model M1.

Fig. 24(b) compares individual turbine efficiencies $\eta_{ind} = P(\gamma = \gamma^*)/P(\gamma = 0)$ from this study, obtained with FLORIS, to those reported in Bempedelis et al. (2023) using LF/LES simulations. Since turbine power scales as $P \sim U^3$, and wind speeds increase downstream (Fig. 22(a)), η_{ind} also increases downstream. This behavior is further explained by the fact that turbines located farther downstream are affected by a larger number of upstream turbines, and therefore by a greater number of wakes. As each upstream turbine applies individual yaw control to mitigate wake effects, the downstream turbines benefit from these adjustments, improving their efficiency. The higher efficiency in the yawed scenario for turbines 2 to 10 is due to increased wind speeds compared to the unyawed scenario, as shown in Fig. 22(a). Optimal yaw control maintains higher wind velocities across turbines, key to increasing power generation.

Notably, the efficiencies of turbines 2 and 3 exceed the expected trend. This deviation results from the significant yaw angles of turbines 1 and 2, which redirect their wakes and minimize overlap with the rotor swept area of turbines 2 and 3. This effect is illustrated by the simulated velocity fields at turbine 2 ($x = 7D$) for both yawed and unyawed cases, as shown in Figs. 25(a) and 25(b), where turbine 2 is indicated with dashed black lines in the unyawed case.

Overall, the yaw control strategy based on model M1 achieves a more uniform power distribution across turbines, reducing the risk of overloading some while underutilizing others. In contrast, the model in Bempedelis et al. (2023) shows a gradual increase in power gain from upstream to downstream turbines.

4. Conclusions

This study investigated the aerodynamic interference between two offshore wind turbines across various operational scenarios using wind

```
% Parameters:
% x1, y1: Coordinates of the upstream turbine.
% H: Hub height of the turbine.
% D: Rotor diameter of the turbine.
% ws: Wind speed.
% wd: Wind direction.
% TI: Turbulence intensity.
% x2, y2: Coordinates of the downstream turbine.

1. Initialize:
- Import libraries and set working directory.
- Initialize variables for results and tracking.

2. Set simulation conditions:
- Wind data: TI, ws, wd.
- Turbine data: H, D, rated wind speed.
- Layout: x1, y1 (upstream), x2, y2 (downstream).

3. Configure:
- Use Gauss-Curl Hybrid wake model.
- Select optimization method (SR, SCIPY, or M1).

4. Simulate and optimize yaw angles:
FOR each turbine model:
  - Compute derived parameters (e.g., D/H ratio).
  FOR each (x2, y2):
    FOR each wind speed (ws):
      - Reinitialize simulation parameters.
        IF SR THEN: Use Serial-Refine method.
        ELSE IF SCIPY THEN: Use SLSQP method.
        ELSE IF M1 THEN: Use regression model.
        - Save computation time.

5. Output:
- Print optimal yaw angles and computation time.
```

Fig. 20. Pseudocode for yaw angle optimization process.

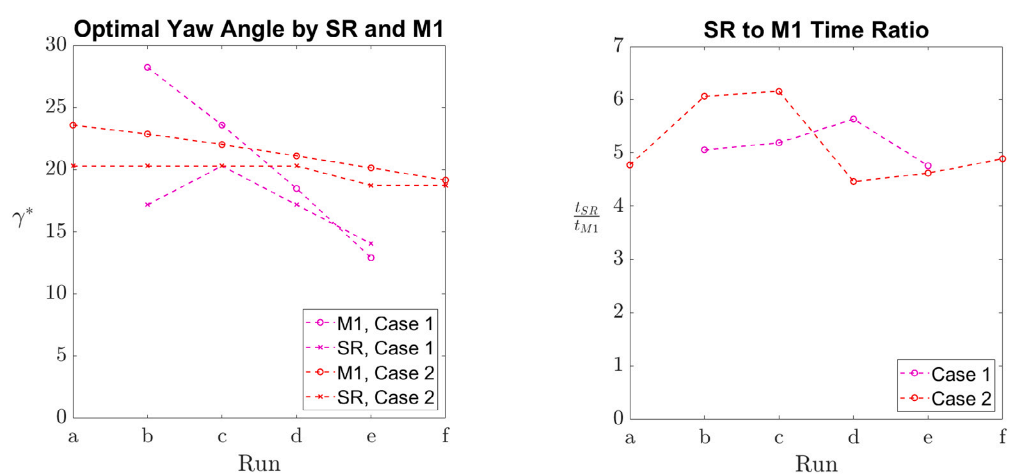

(a) (b)

Fig. 21. Comparison of model M1 and SR method performance in Case 1 and Case 2: (a) Optimal yaw angles, (b) Computational time ratio.

farm simulation software. Numerous numerical simulations were conducted, considering different wind speeds, turbulence intensities, turbine models, orientations, and layouts. Two regression models were developed: one to estimate the optimal yaw angle of the upstream turbine for maximizing power generation and another to assess the percentage power gain achievable through active yaw control. Additionally, a decision tree-based classification model was designed to determine the necessity of turbine reorientation based on operational conditions.

The decision tree achieved a high accuracy rate of 96.11%, making it suitable for identifying when turbine orientation adjustments are necessary. Redirection was essential particularly when the downstream turbine was at a positive spanwise distance and wind speed was below

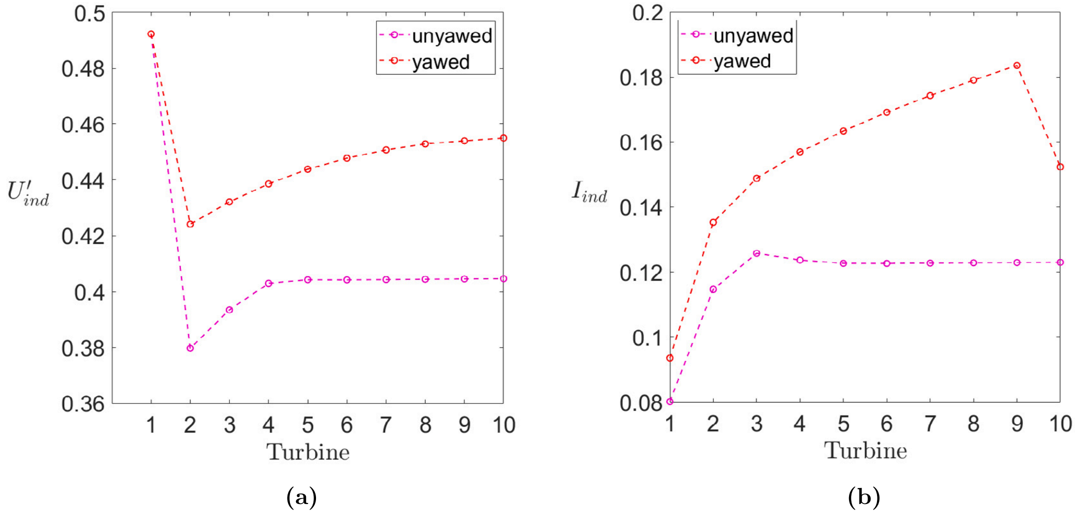

Fig. 22. Local turbine wind conditions in the yawed and unyawed scenarios: (a) Dimensionless wind velocity, (b) Turbulence intensity.

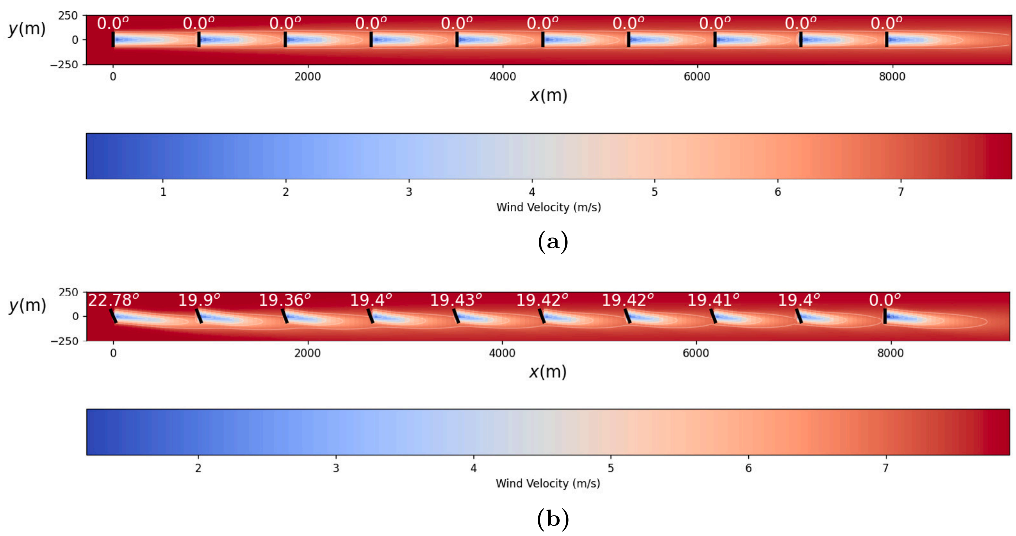

Fig. 23. Simulated velocity fields at turbine hub height (horizontal cut) for Case 3 conditions: (a) Unyawed turbines, (b) Yawed turbines.

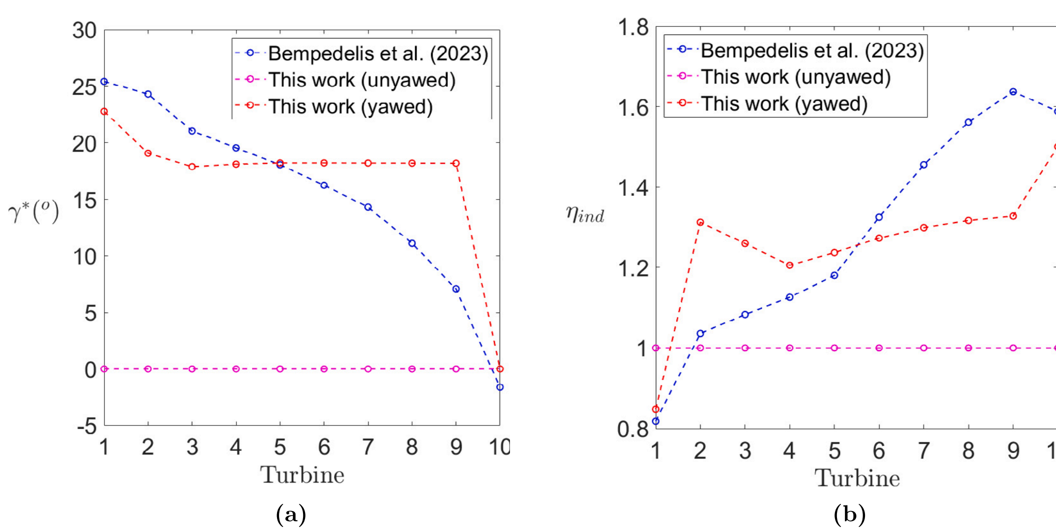

Fig. 24. Comparison of results between this study and Bempedelis et al. (2023): (a) Optimal yaw angle, (b) Individual turbine efficiency.

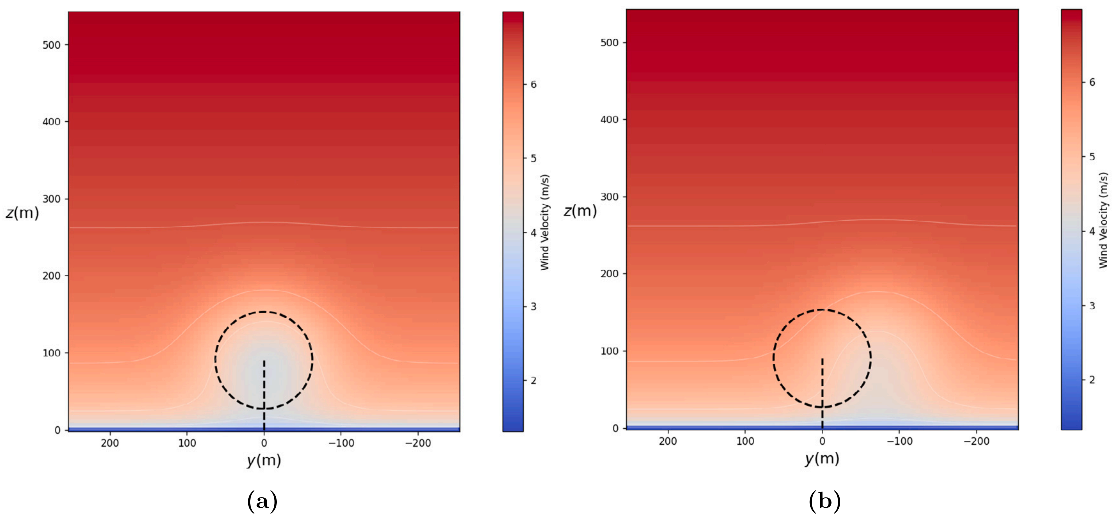

Fig. 25. Simulated velocity fields at $x = 7D$ (vertical cross-section) under Case 3 conditions: (a) Unyawed turbines, (b) Yawed turbines.

120% of the nominal turbine speed. Shorter distances between turbines and lower turbulence intensities increased the need for upstream turbine redirection to mitigate wake-induced power losses.

The ratio of spanwise to streamwise distance between turbines was the most significant factor in estimating the optimal yaw angle, followed by the absolute distance between turbines and wind turbulence intensity. The estimation error decreased with greater distances between turbines, averaging 8.7% for distances of 5.0062 rotor diameters or more. The optimal yaw angle regression model showed good agreement with simulation results.

Wind turbulence intensity had the most significant impact on the percentage power gain, followed by the spanwise to streamwise distance ratio and wind speed. The distance between turbines had a lesser effect. The highest power gain occurred when the spanwise distance was approximately 4% of the streamwise distance. Although the power gain regression model followed the trend of the simulations, its high errors suggest it is suitable for qualitative analysis rather than precise predictions. Simulations showed that optimal yaw control under the studied conditions could achieve up to a 25.6% power gain.

The regression models in this study are based on simulation results obtained with FLORIS. While FLORIS incorporates velocity deficit models, wake deflection models, and wake interference effects, which have been continually refined and align well with experimental data, higher-fidelity models exist. For example, SOWFA (Simulator for Wind Farm Applications), which uses LES, captures wind physics within a wind farm more accurately than FLORIS, though it is computationally more intensive. SOWFA could be used as a foundational tool to develop regression models that achieve greater accuracy. The lower accuracy of the optimal yaw angle regression model for short turbine spacings, specifically near the boundary of the near-wake region (about five rotor diameters), can be attributed to the limitations of FLORIS, particularly in accurately predicting wake interactions at these distances.

Careful consideration of farm layout, wind conditions, and turbine characteristics is crucial for selecting effective yaw control strategies. Yaw control is more beneficial in dense wind farms with lower turbine spacing, particularly under mild wind conditions. The developed models eliminate the need for resource-intensive simulations, demonstrating computational efficiency and enabling swift, reasonably accurate estimation of optimal turbine yaw angles. This facilitates rapid parametric studies and online power optimization.

Model M1 demonstrated greater computational efficiency compared to previous optimization methods and, when combined with model M0, can facilitate yaw control across a wind farm, yielding a relatively uniform distribution of yaw angles and turbine efficiencies. This uniformity is beneficial for managing wind loads and contributes positively to turbine operation. Future work will involve testing these models on a larger scale within a wind farm featuring multiple turbines and assessing their performance under deep array effects. Developing a computational framework to regulate the yaw angles of all interacting turbines will be imperative.

5. List of symbols

a_i, b_i: ith coefficient of the regression models
D: rotor diameter of the wind turbine, m
$d = \sqrt{x^2 + y^2}$: distance between wind turbines, m
$d' = d/D$: dimensionless distance between wind turbines
H: hub height of the wind turbine, m
I: wind turbulence intensity, %
P_r: rated power of the wind turbine, MW
r^2: coefficient of determination of the fit
t_{M1}: computational time recorded for model M1, s
t_{SR}: computational time recorded for the SR method, s
U: wind speed, m/s
$U' = U/U_r$: dimensionless wind speed
U_a: wind turbine cut-in speed, m/s
U_c: wind turbine cut-out speed, m/s
U_r: rated wind speed of the wind turbine, m/s
x: streamwise distance between wind turbines, m
y: spanwise distance between wind turbines, m
$y' = y/x$: spanwise-to-streamwise distance ratio

Subscripts
γ^*: referring to the optimal yaw angle of the wind turbine
0: referring to a wind turbine yaw angle equal to zero
b: referring to a binary variable
ΔP: referring to the power gain associated with wind turbine yaw control
ind: denotes an individual turbine

Superscripts
$*$: referring to the optimum

Greek Letters
γ: yaw angle of the upstream wind turbine,^{o}
γ^*: optimal yaw angle of the upstream wind turbine,^{o}
γ_b: binary response of the classifier model
ΔP: power gain associated with wind turbine yaw control, %
$\Delta\gamma_i^*$: absolute maximum change in γ^* resulting from a change in predictor i,^{o}

ϵ_{γ^*}: error in wind turbine orientation between model and simulations, %

$\epsilon_{\Delta P}$: error in power gain between model and simulations, %

$\eta = \sum_{i=1}^{N} P_i(\gamma = \gamma^*) / \sum_{i=1}^{N} P_i(\gamma = 0°)$: turbine efficiency

Acronyms

AYC: Active yaw control
BO: Bayesian Optimization
FLORIS: FLOw Redirection and Induction in Steady State
GCH: Gauss-Curl-Hybrid
GS: Grid Search
LES: Large eddy simulations
LES-BO: Large Eddy Simulation with Bayesian Optimization
LF/LES: Low-Fidelity model combined with Large Eddy Simulation (LES)
M0: Classification model
M1: Regression model for the optimal yaw angle of the wind turbine
M2: Regression model for the percentage power gain
NREL: National Renewable Energy Laboratory
PSO: Particle Swarm Optimization
RII: Relative Importance Index
RS: Random Search
SCADA: Supervisory Control and Data Acquisition
SLSQP: Sequential Least Squares Programming
SOWFA: Simulator fOr Wind Farm Applications
SR: Serial-Refine method
T1: Upstream wind turbine
T2: Downstream wind turbine

Funding

The author did not receive financial support for the research, authorship, and/or publication of this article.

Declaration of competing interest

The authors declare that they have no known competing financial interests or personal relationships that could have appeared to influence the work reported in this paper.

References

Aju, Emmanuvel Joseph, Kumar, Devesh, Leffingwell, Melissa, Rotea, Mario A, Jin, Yaqing, 2023. The influence of yaw misalignment on turbine power output fluctuations and unsteady aerodynamic loads within wind farms. Renew. Energy 215, 118894.

Amiri, Mojtaba Maali, Shadman, Milad, Estefen, Segen F., 2024. A review of physical and numerical modeling techniques for horizontal-axis wind turbine wakes. Renew. Sustain. Energy Rev. 193, 114279.

Annoni, Jennifer, Fleming, Paul, Scholbrock, Andrew, Roadman, Jason, Dana, Scott, Adcock, Christiane, Porte-Agel, Fernando, Raach, Steffen, Haizmann, Florian, Schlipf, David, 2018. Analysis of control-oriented wake modeling tools using lidar field results. Wind Energy Sci. 3 (2), 819–831.

Archer, Cristina L., Vasel-Be-Hagh, Ahmad, 2019. Wake steering via yaw control in multi-turbine wind farms: Recommendations based on large-eddy simulation. Sustain. Energy Technol. Assess. 33, 34–43.

Bastankhah, Majid, Porté-Agel, Fernando, 2016. Experimental and theoretical study of wind turbine wakes in yawed conditions. J. Fluid Mech. 806, 506–541.

Bastankhah, Majid, Porté-Agel, Fernando, 2019. Wind farm power optimization via yaw angle control: A wind tunnel study. J. Renew. Sustain. Energy 11 (2).

Bempedelis, Nikolaos, Gori, Filippo, Wynn, Andrew, Laizet, Sylvain, Magri, Luca, 2023. Data-driven optimisation of wind farm layout and wake steering with large-eddy simulations. Wind Energy Sci. Discuss. 2023, 1–23.

Boveri, Asea Brown, Abb, S., 2012. Cuaderno De Aplicaciones Técnicas N. 12 Plantas Eólicas. Barcelona, España.

Ciri, Umberto, Rotea, Mario A., Leonardi, Stefano, 2018. Effect of the turbine scale on yaw control. Wind Energy 21 (12), 1395–1405.

Das, Rubel C., Shen, Yu-Lin, 2023. Analysis of wind farms under different yaw angles and wind speeds. Energies 16 (13), 4953.

Doekemeijer, Bart Matthijs, Simley, Eric, Fleming, Paul, 2022. Comparison of the Gaussian wind farm model with historical data of three offshore wind farms. Energies 15 (6), 1964.

Fleming, Paul A, Gebraad, Pieter MO, Lee, Sang, van Wingerden, Jan-Willem, Johnson, Kathryn, Churchfield, Matt, Michalakes, John, Spalart, Philippe, Moriarty, Patrick, 2014. Evaluating techniques for redirecting turbine wakes using SOWFA. Renew. Energy 70, 211–218.

Fleming, Paul, Sinner, Michael, Young, Tom, Lannic, Marine, King, Jennifer, Simley, Eric, Doekemeijer, Bart, 2021. Experimental results of wake steering using fixed angles. Wind Energy Sci. Discuss. 2021, 1–18.

Fleming, Paul A, Stanley, Andrew PJ, Bay, Christopher J, King, Jennifer, Simley, Eric, Doekemeijer, Bart M, Mudafort, Rafael, 2022. Serial-refine method for fast wake-steering yaw optimization. In: Journal of Physics: Conference Series. Vol. 2265, IOP Publishing, 032109.

Gaertner, Evan, Rinker, Jennifer, Sethuraman, Latha, Zahle, Frederik, Anderson, Benjamin, Barter, Garrett E, Abbas, Nikhar J, Meng, Fanzhong, Bortolotti, Pietro, Skrzypinski, Witold, et al., 2020. IEA Wind TCP Task 37: Definition of the IEA 15-megawatt offshore Reference Wind Turbine. Technical Report, National Renewable Energy Lab.(NREL), Golden, CO (United States).

Gori, Filippo, Laizet, Sylvain, Wynn, Andrew, 2023. Sensitivity analysis of wake steering optimisation for wind farm power maximisation. Wind Energy Sci. Discuss. 2023, 1–33.

He, Ruiyang, Yang, Hongxing, Lu, Lin, Gao, Xiaoxia, 2024. Site-specific wake steering strategy for combined power enhancement and fatigue mitigation within wind farms. Renew. Energy 225, 120324.

He, Ruiyang, Yang, Hongxing, Sun, Shilin, Lu, Lin, Sun, Haiying, Gao, Xiaoxia, 2022. A machine learning-based fatigue loads and power prediction method for wind turbines under yaw control. Appl. Energy 326, 120013.

Howland, Michael F., Lele, Sanjiva K., Dabiri, John O., 2019. Wind farm power optimization through wake steering. Proc. Natl. Acad. Sci. 116 (29), 14495–14500.

Jensen, Niels Otto, 1983. A Note on Wind Generator Interaction. Risø National Laboratory.

Jiménez, Ángel, Crespo, Antonio, Migoya, Emilio, 2010. Application of a LES technique to characterize the wake deflection of a wind turbine in yaw. Wind Energy 13 (6), 559–572.

Jonkman, Jason, Butterfield, Sandy, Musial, Walter, Scott, George, 2009. Definition of a 5-MW Reference Wind Turbine for Offshore System Development. Technical Report, National Renewable Energy Lab.(NREL), Golden, CO (United States).

Kim, Minjeong, Lim, Hyeyeong, Park, Sungsu, 2023. Comparative analysis of wind farm simulators for wind farm control. Energies 16 (9), 3676.

King, Jennifer, Fleming, Paul, King, Ryan, Martínez-Tossas, Luis A, Bay, Christopher J, Mudafort, Rafael, Simley, Eric, 2021. Control-oriented model for secondary effects of wake steering. Wind Energy Sci. 6 (3), 701–714.

Kumar, Devesh, Rotea, Mario A, Aju, Emmanuvel J, Jin, Yaqing, 2023. Wind plant power maximization via extremum seeking yaw control: A wind tunnel experiment. Wind Energy 26 (3), 283–309.

Kuo, Jim, Pan, Kevin, Li, Ni, Shen, He, 2020. Wind farm yaw optimization via random search algorithm. Energies 13 (4), 865.

Li, Baoliang, He, Jia, Ge, Mingwei, Ma, Hongliang, Du, Bowen, Yang, Haoze, Liu, Yongqian, 2022. Study of three wake control strategies for power maximization of offshore wind farms with different layouts. Energy Convers. Manage. 268, 116059.

Lin, Mou, Porté-Agel, Fernando, 2020. Power maximization and fatigue-load mitigation in a wind-turbine array by active yaw control: An LES study. In: Journal of Physics: Conference Series. Vol. 1618, IOP Publishing, 042036.

Niayifar, Amin, Porté-Agel, Fernando, 2016. Analytical modeling of wind farms: A new approach for power prediction. Energies 9 (9), 741.

Ozbay, Ahmet, Tian, Wei, Yang, Zifeng, Hu, Hui, 2012. Interference of wind turbines with different yaw angles of the upstream wind turbine. In: 42nd AIAA Fluid Dynamics Conference and Exhibit. p. 2719.

Pei, Yan, Qian, Zheng, Jing, Bo, Kang, Dahai, Zhang, Lizhong, 2018. Data-driven method for wind turbine yaw angle sensor zero-point shifting fault detection. Energies 11 (3), 553.

Sadan, Milan K., Ahn, Hyo-Jun, Chauhan, G.S., Reddy, N.S., 2016. Quantitative estimation of poly (methyl methacrylate) nano-fiber membrane diameter by artificial neural networks. Eur. Polym. J. 74, 91–100.

Simley, Eric, Fleming, Paul, Girard, Nicolas, Alloin, Lucas, Godefroy, Emma, Duc, Thomas, 2021. Results from a wake steering experiment at a commercial wind plant: investigating the wind speed dependence of wake steering performance. Wind Energy Sci. Discuss. 2021, 1–39.

Song, Jeonghwan, Kim, Taewan, You, Donghyun, 2023. Particle swarm optimization of a wind farm layout with active control of turbine yaws. Renew. Energy 206, 738–747.

Stanley, Andrew P.J., Bay, Christopher J., Fleming, Paul, 2023. Enabling control co-design of the next generation of wind power plants. Wind Energy Sci. 8 (8), 1341–1350.

Stanley, Andrew PJ, Bay, Christopher, Mudafort, Rafael, Fleming, Paul, 2022. Fast yaw optimization for wind plant wake steering using Boolean yaw angles. Wind Energy Sci. 7 (2), 741–757.

Stegner, Alexandre, Drobinski, Philippe, Plougoven, Riwal, Haeffelin, Martial, Wind resources for renewable energies. https://www.coursera.org/learn/wind-for-renewable-energies (Accessed 9 May 2024).

van Beek, Maarten T., Viré, Axelle, Andersen, Søren J., 2021. Sensitivity and uncertainty of the floris model applied on the lillgrund wind farm. Energies 14 (5), 1293.

Wei, Dezhi, Wang, Nina, Wan, Decheng, Strijhak, Sergei, 2023. Parametric study of the effectiveness of active yaw control based on large eddy simulation. Ocean Eng. 271, 113751.

Xin, Zhiqiang, Liu, Songyang, Cai, Zhiming, Liao, Shenghai, Huang, Guoqing, 2022. Numerical study on the yaw control for two wind turbines under different spacings. Appl. Sci. 12 (14), 7098.

Zong, Haohua, Enbo, Sun, 2022. Reivew of active wake control for horizontal-axis wind turbines. Acta Aerodyn. Sinica 40 (4), 51–68.

Zong, Haohua, Porté-Agel, Fernando, 2021. Experimental investigation and analytical modelling of active yaw control for wind farm power optimization. Renew. Energy 170, 1228–1244.